

# A new frontier of flexible energy devices: Aqueous proton supercapacitors

Cite as: Appl. Phys. Rev. 11, 011301 (2024); doi: 10.1063/5.0172379

Submitted: 15 August 2023 · Accepted: 13 December 2023 ·

Published Online: 16 January 2024



Jing Liang  and Wei Wu<sup>a)</sup> 

## AFFILIATIONS

Laboratory of Printable Functional Materials and Printed Electronics, School of Physics and Technology, Wuhan University, Wuhan 430072, People's Republic of China

<sup>a)</sup>Author to whom correspondence should be addressed: [weiwu@whu.edu.cn](mailto:weiwu@whu.edu.cn)

## ABSTRACT

Aqueous proton supercapacitors are considered as promising energy storage devices for next-generation wearable electronics due to their high energy density, rapid kinetics, long cycles, and reliable safety. As of now, the research for electrochemical proton energy storage entails more holistic considerations. In this review, we provide a timely and comprehensive review of recent advances in electrochemical proton storage. First, we discuss the main explored proton storage electrode materials, including carbon materials, metal oxides, Prussian blue, COFs, and MXenes, from the aspects of structure, preparation strategy, and proton storage mechanism. Furthermore, we systematically focus on their multifunctional applications of proton supercapacitors including flexible and wearable electronics, anti-freezing energy storage system, etc. Finally, the challenges and prospects of flexible proton supercapacitors are outlined. We believe that this review will greatly improve the knowledge of proton energy storage and facilitate the development of advanced electrochemical energy systems.

Published under an exclusive license by AIP Publishing. <https://doi.org/10.1063/5.0172379>

## TABLE OF CONTENTS

I. INTRODUCTION.....	1
II. ELECTROCHEMICAL PROTON STORAGE.....	2
III. ELECTROCHEMICAL PROTON STORAGE MATERIALS .....	3
A. Positive electrode materials .....	3
1. Carbon materials.....	3
2. Prussian blue analogs.....	5
3. Covalent organic frameworks.....	6
4. Miscellaneous materials .....	6
B. Negative electrode materials .....	7
1. Tungsten oxides .....	7
2. Molybdenum oxides.....	7
3. Vanadium oxides .....	7
4. MXenes.....	8
5. Other materials .....	9
IV. PROTON STORAGE BASED FLEXIBLE SUPERCAPACITORS .....	10
V. CONCLUSION AND PERSPECTIVES .....	11

## I. INTRODUCTION

The rapid development of Internet of Things technology has prompted various intelligent portable and wearable electronics which

has been gradually entered people's daily life, with a wide range of applications, including personal healthcare, smart home, electronic skin, etc.<sup>1,2</sup> According to statistics, the global market of flexible electronics will reach  $300 \times 10^9$  dollars by 2025. However, powering these growing number of flexible electronics is a challenge because of the urgent and huge demand for flexibility and small device size ( $<10$  cm).<sup>3</sup> Lithium-ion batteries (LIBs) have been considered as a prevailing solution owing to their high energy sustainability and power reliability.<sup>3,4</sup> Recently, some promising LIBs also have been explored to achieve higher energy density, such as Li-S batteries,<sup>5,6</sup> Li-CO<sub>2</sub> batteries,<sup>7</sup> and Li-O<sub>2</sub> batteries.<sup>8</sup> Despite lithium-ion based batteries deliver high energy density, their development is still hampered by limited flexibility, low power density, and limited safety.

In this regard, extensive efforts have been devoted to other metal charge carriers-based aqueous batteries and supercapacitors, such as K<sup>+</sup>,<sup>9,10</sup> Na<sup>+</sup>,<sup>11</sup> and Zn<sup>2+</sup>.<sup>12</sup> To date, these charge carriers not only offer advantages of rich resources and high safety, but also can transport more charges. Although metal-ion batteries have many advantages, challenges such as unstable reactivity, large volume expansion, and dendrite growth hinder their further application. Until now, researchers have made various effective tactics to solve these issues, including designing novel electrode materials, developing gel polymer electrolyte, etc. Notably, the development of gel polymer electrolyte has been reported as an efficient strategy to impede the dendrite

growth. For instance, Bella and his group designed a UV-cured gel electrolyte and a biosourced polymer electrolyte with mechanical robustness for potassium batteries, showing stable cycle properties up to 600 cycles.<sup>13,14</sup> Moreover, the large solvation radius of metallic ions can limit the fast charge transport. Therefore, a charge carrier with smaller ionic radius could lead to higher electron transport kinetics. Apart from aqueous batteries, supercapacitors or sustainable supercapacitors have attracted extensive attention in the field of flexible applications, due to intrinsic safety, low cost, and small size.<sup>15</sup> In this regard, integrating nonmetal ion charge carriers with supercapacitors becomes an effective strategy to manufacture novel types of energy storage devices that offer high energy and power density.

The proton ( $H^+$ ) has smallest radius and lowest weight and is considered as a new type of charge carrier.<sup>16–18</sup> Compared with lithium/sodium carriers, proton delivers strong vitality for high energy density and power density due to its advantages of lower adsorption and desorption barrier and faster surface interface reaction in the acid electrolyte. In recent years, some excellent proton electrode materials have been explored, including two-dimensional materials and hydrated metal oxides. For instance, the transition metal carbides (MXenes) can provide a high capacitance of  $210\text{ F g}^{-1}$  at a scan rate of  $10\text{ V s}^{-1}$  in the  $3\text{ M H}_2\text{SO}_4$  electrolyte, which is better than that of all carbon materials or transition metal oxides.<sup>19</sup> In addition, the proton possesses a smaller hydrated ionic size ( $2.82\text{ \AA}$ ) than  $[\text{Zn}(\text{H}_2\text{O})_6]^{2+}$  ( $5.5\text{ \AA}$ ), which can significantly enhance the ion migration rate and reaction kinetics of protons.<sup>20</sup> Typically, in terms of  $\text{MoO}_3$  electrode materials, the theoretical specific capacity of the  $\text{HMnO}_3$  electrode can reach  $185\text{ mAh g}^{-1}$ , which is higher than the  $\text{LiMoO}_3$  ( $177\text{ mAh g}^{-1}$ ) and  $\text{NaMoO}_3$  ( $160\text{ mAh g}^{-1}$ ). Furthermore, the  $\text{MoO}_3$  electrodes demonstrate a low activation energy ( $E_a$ ) of  $0.28\text{ eV}$ , which belongs to the Grotthuss conduction mechanism ( $E_a < 0.4\text{ eV}$ ).<sup>21</sup> The hydrogen-bonding network in the  $\text{MoO}_3$  electrode provides high-kinetics charge carrier diffusion, implying that the selective  $\text{H}_3\text{O}$ -intercalation chemistry can fabricate the electrodes with long cycle life and large specific capacity. Nowadays, the research on proton carrier-based supercapacitors has attracted many attention and has obtained certain development. However, a thorough understanding review for proton-based flexible supercapacitors remains limited.

Overall, electrochemical proton storage provides new technical opportunities for manufacturing high performance flexible supercapacitors. Several reviews have discussed the recent developments in the field of proton batteries;<sup>17</sup> however, a deeper and comprehensive understanding of the electrode materials, charge storage mechanism of proton-insertion energy storage in supercapacitors has not been reviewed to date. We, therefore, provide a timely and comprehensive review of recent progress in electrochemical proton storage. First, we systematically discussed the explored electrode materials for proton storage in terms of structure, fabrication strategies, and mechanism, including metal oxide, PBAs, COFs, MXenes, etc. Moreover, we focus on the latest advanced applications of proton supercapacitors, including wearable electronics, anti-freezing energy storage, and sensing system. Finally, based on the challenge and prospect, we aim to provide new insight into future research direction, including the guidelines for electrode materials design, low-cost production, and integration prospect.

## II. ELECTROCHEMICAL PROTON STORAGE

The energy storage mechanism of supercapacitors mainly depends on the surface-capacitance effect, thereby exhibiting high

power density. Therefore, supercapacitors are classified into electric double layer supercapacitors (EDLCs), pseudocapacitors, and hybrid supercapacitors according to their energy storage mechanisms. Among the EDLCs, the charges are main physical adsorbed and accumulated on both sides of the electrode/electrolyte interface. The most typical material includes carbon material, such as activated carbon and graphene. Pseudocapacitors introduce redox or Faraday reaction at or near the surface of electrode, breaking the restrictions of the surface area, and thus exhibiting enhanced capacitance. The hybrid supercapacitors combine the advantages of EDLCs and pseudocapacitors. Flexible solid-state supercapacitors are considered as the promising candidates for the next-generation lightweight, wearable, and portable electronics. To sum up, the main determinant of the ability of supercapacitors to store energy is the interaction between charge carriers and electrode materials. Therefore, it is best to understand the process of carrier at the interface between the electrolyte solvent and the electrode material. Among various charge carriers ( $K^+$ ,  $\text{Na}^+$ ,  $\text{Li}^+$ , etc.), proton or hydrogen ( $H^+$ ) is a promising candidate that enables the prosperity for FSCs due to its faster ions-insertion rate, smallest radius, lowest ionic weight, as depicted in Fig. 1(a).<sup>22,23</sup> In 1806, the proton transportation mechanism was first defined as the Grotthuss mechanism, which is similar to Newton's cradle, as shown in Fig. 1(b). Furthermore, the protons can be reversibly inserted-into/extract-from the electrode materials due to its small size and light weight. Therefore, ideal electrode materials for proton storage should possess wide channels. In recent years, many electrode materials with tunnel structure, layer structure, and open-framework structure have been fabricated and explored as large-channel materials [Fig. 1(c)], such as  $\text{RuO}_2$ ,  $\text{MoO}_3$ , PBAs, and MXenes. From the literature, the proton energy storage mechanism can be divided into two types: a surface redox reaction mechanism and an intercalation reaction mechanism [Fig. 1(d)]. Section III mainly discusses the electrochemical performance and proton storage mechanism of the developed electrode materials based on the positive and negative electrodes.

In general, the electrode materials reversible store proton or hydrogen ion in acid electrolyte based on the Grotthuss mechanism. Therefore, the electrolyte used for proton energy storage is mainly acid solutions, including  $\text{H}_2\text{SO}_4$ ,  $\text{H}_3\text{PO}_4$ , etc.<sup>24</sup> However, the proton exists in the form of  $\text{H}_3\text{O}^+$  in acid solution due to the high de-solvation energy bonded by  $\text{H}_2\text{O}$  solvents ( $11.66\text{ eV}$ ). Compared with other metal ions, the hydrated proton ions ( $\text{H}_3\text{O}^+$ ) demonstrated a smaller radius and can be inserted into the electrode materials. Phosphoric acid ( $\text{H}_3\text{PO}_4$ ) is also considered as a promising proton electrolyte to produce  $\text{H}^+$ , as well as the Brønsted-Lowry acid-base substance.<sup>25</sup> Furthermore, although some exciting research results have been achieved in developing electrode materials with outstanding electrochemical performance, the occurrence of hydrogen evolution reaction and the corrosion of electrode materials in the acid electrolyte also need to be valuable for the fabrication of proton-based supercapacitors devices.

The flourishing of the development on proton-based supercapacitors has been achieved in recent years. However, proton-based supercapacitors still face challenges in further practical applications, such as incomplete understanding of energy storage mechanism, uncontrollable corrosion of electrode materials in acidic electrolyte, and the high freezing point of electrolytes.<sup>26</sup> For example, the Grotthuss mechanism has been observed in many electrode materials, such as PBAs, MXenes and others. Interestingly, this phenomenon is not observed in

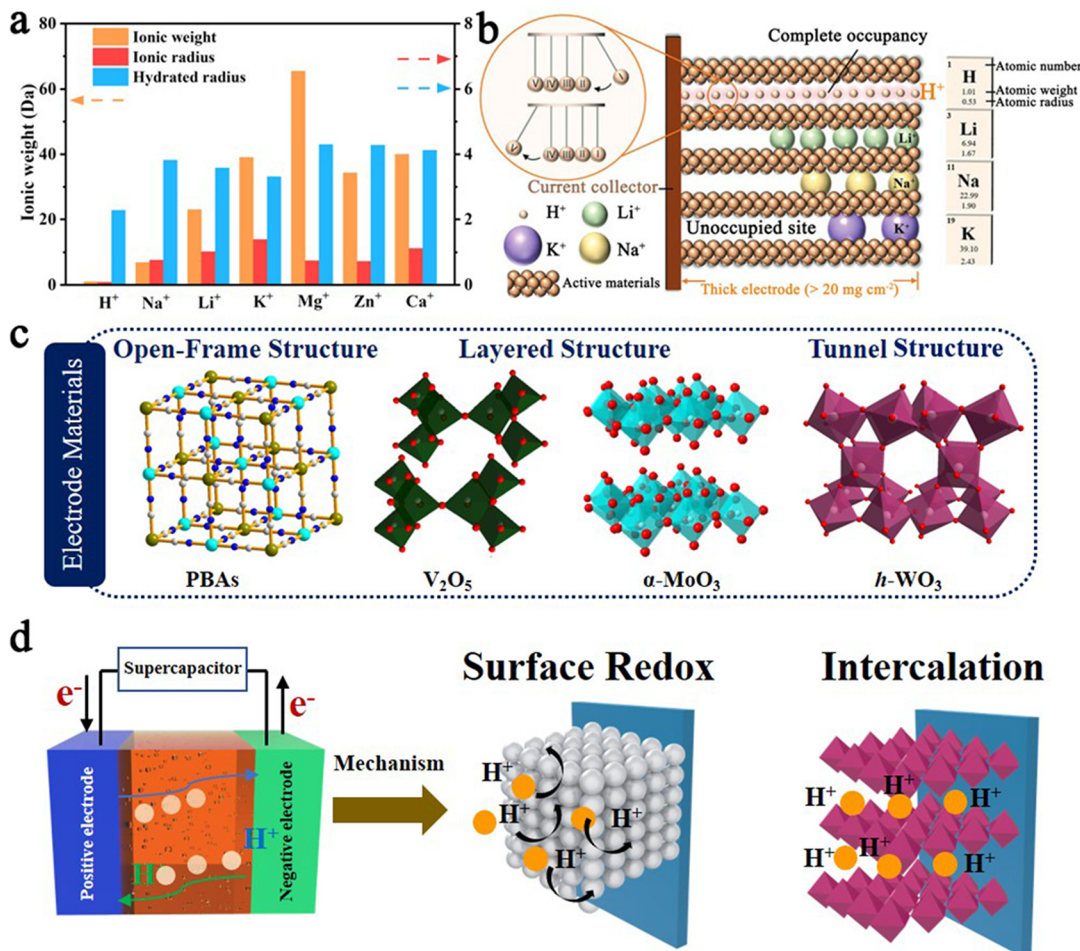


**FIG. 1.** Physicochemical properties, electrode materials, and charge storage mechanisms of proton charge carriers. (a) Ionic weight, ionic radius, and hydrated radius for typical cation charge carriers. (b) Schematic illustration of the diffusion of different charge carriers in electrodes, in which protons demonstrate fastest transport rate. Reproduced with permission from Su *et al.*, *Adv. Funct. Mater.* **30**(46), 2005477 (2020). Copyright 2020 Wiley-VCH Verlag GmbH & Co. KGaA.<sup>29</sup> (c) The typical electrode materials for proton energy storage. (d) Schematic illustration of the mechanism for proton-based supercapacitors.

the  $\text{WO}_3 \cdot 2\text{H}_2\text{O}$  and hexagonal  $\text{WO}_3 \cdot 0.6\text{H}_2\text{O}$ . By monitoring the mass changes via Electrochemical Quartz Crystal Microbalance (EQCM), it has been confirmed that proton migration in the  $\text{WO}_3$  electrode is mediated by bridge oxygens during first cycling, instead of through Grotthuss mechanism.<sup>27</sup> In addition, proton-based supercapacitors typically utilized acidic electrolytes because protons act as the charge carriers. Likewise, corrosion of  $\text{MoO}_3$  has also been observed in the acid electrolyte. For instance, the capacity of  $\text{MoO}_3$  decreased to 68% of its initial value only after 100 cycles in the protonation insertion process.<sup>28</sup> Proton-based supercapacitors often use aqueous electrolytes, which have a relatively high freezing point compared to organic or ionic liquid electrolytes. This high freezing point can limit the operation of proton-based supercapacitors in cold environments.

Under these effects, the proton-based energy storage devices tend to exhibit shorter lifetimes and narrower potential windows. Comfortingly, to date, considerable efforts have been devoted to

develop high-performance proton-based supercapacitors. Recent strategies can be mainly summarized as designing electrode materials, exploring advanced characterization techniques, modifying electrolyte, and developing hybrid device that combine proton supercapacitor with batteries. We will discuss these progresses and provide a thorough understanding review for proton-based flexible supercapacitors in this work.

### III. ELECTROCHEMICAL PROTON STORAGE MATERIALS

#### A. Positive electrode materials

##### 1. Carbon materials

The carbon materials are one of the representative positive electrodes of proton supercapacitors.<sup>30</sup> The positive carbon electrode materials usually demonstrated excellent electrochemical

characteristics, such as large specific surface area, high working voltage, good conductivity, and strong wettability. Until now, carbon-based positive materials have been widely studied, including activated carbon, graphene, carbon nanotubes, and other carbon-based materials.<sup>31</sup> Activated carbon, as the earliest reported positive electrode material for capacitors, still receives widespread attention due to its simple synthesis process, abundant raw materials, and low price. Activated carbon is a carbon material with rich pore structure obtained from organic raw materials through high-temperature heat treatment or acid/alkali treatment. The pore structure and chemical composition of activated carbon mainly depend on the precursor, activator, and preparation method. By rationally adjusting the preparation process, the specific surface area, pore structure, and doping elements suitable for double layer adsorption/pseudocapacitance can be obtained. For instance, Hatori *et al.* first discovered that the nitrogen-rich carbon has high pseudocapacitance characteristics in  $\text{H}_2\text{SO}_4$  electrolytes.<sup>32</sup> However, the reason why carbon materials can achieve high capacitance in acidic electrolytes is still unclear. To explain the above issues, the researchers calculated the contribution of protons to capacitance,

which is much higher (*ca.* 70%) than that of sulfate ions (*ca.* 30%) by three electrode tests [Figs. 2(a) and 2(b)]. This indicates that carbon materials are prefer to adsorb the protons.<sup>33</sup> To further develop the carbon materials with high energy density, oxygen and nitrogen co-doping strategy is explored to prepared proton-based supercapacitors.<sup>34</sup> As shown in Fig. 2(c), the carbon materials offer a capacitance of  $368 \text{ F g}^{-1}$  at  $1 \text{ mV s}^{-1}$  and a long cycling of 25 000 cycles. The proton-trapping mechanism plays a vital role in outstanding electrochemical performance. Although many carbon materials have been explored in acid electrolytes, the proton mechanism remains confusing. Recently, the proton-intercalation process in carbon materials has been first elucidated. Liu and his group explored carbon materials with superstructures [Figs. 2(d)–2(h)], which delivers fast proton-coupled kinetics, superior capacitance ( $468 \text{ F g}^{-1}$  at  $1 \text{ A g}^{-1}$ ), ultra-long cycle life (1 000 000 cycles), and high-rate capability ( $100 \text{ A g}^{-1}$ ) for carbon-based supercapacitors.<sup>35</sup> It can be concluded that the carbon superstructure is benefit for proton storage and long cyclability. Therefore, this work will stimulate the proton research for carbon materials and holds great promise for efficient proton energy storage.

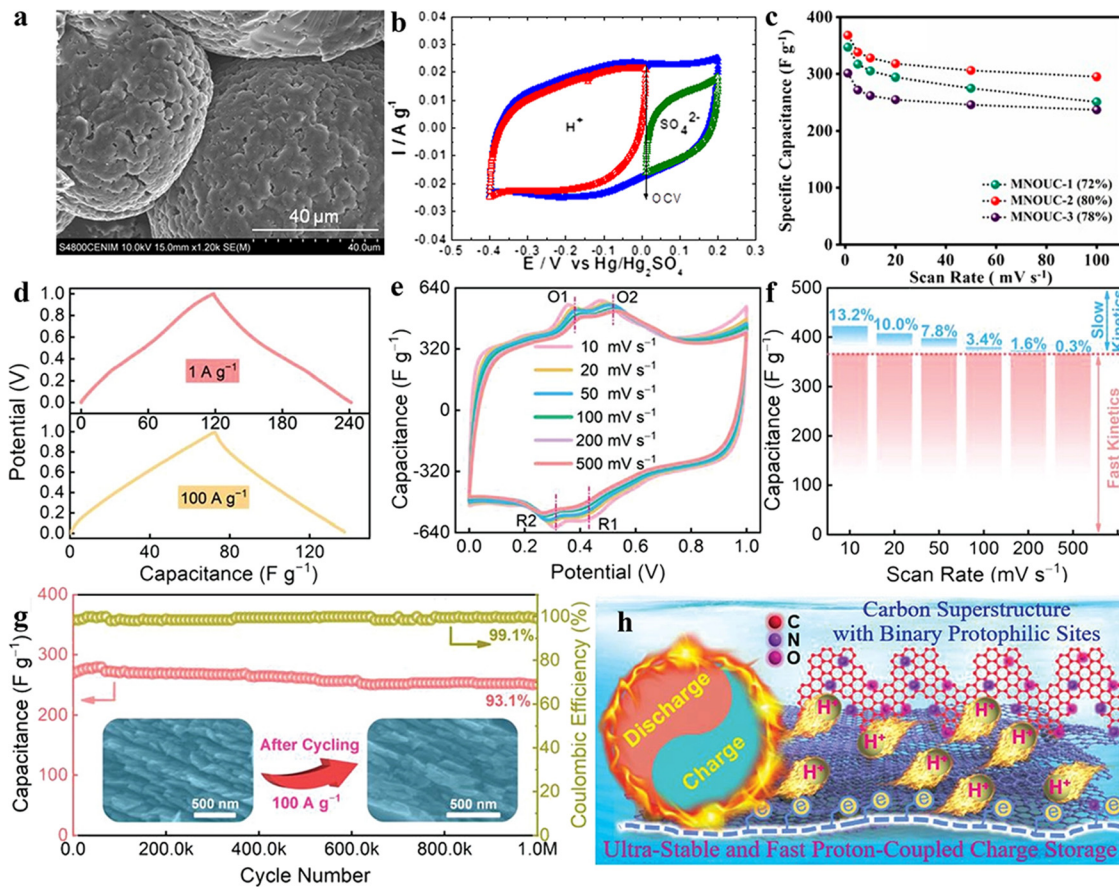


**FIG. 2.** Characterization and electrochemical performance of carbon materials for proton storage. (a) The SEM images, (b) CV, and (c) GCD curves of carbon materials. Reproduced with permission from Barranco *et al.*, J. Power Sources **262**, 23–28 (2014). Copyright 2014 Elsevier;<sup>33</sup> Reproduced with permission from Barua *et al.*, Energy Fuel **35**(12), 10262–10273 (2021). Copyright 2021 American Chemical Society.<sup>34</sup> The (d) GCD, (e) CV curves, (f) capacitance contribution, (g) cycling, and (h) illustration of mechanism of carbon materials with superstructure. Reproduced with permission from Song *et al.*, Adv. Mater. **33**(49), 2104148 (2021). Copyright 2021 Wiley-VCH Verlag GmbH & Co. KGaA.<sup>35</sup>

## 2. Prussian blue analogs

Prussian blue (PB) and its analogs (PBAs) with the molecular formula  $A_2M[Fe(CN)_6] \cdot nH_2O$  ( $A$  is alkali metal ions,  $M$  is transition metal ions) are open-framework materials, which are conducive to proton transport, as shown in Fig. 3(a).<sup>36</sup> First,  $M$ , as a transition metal center, can precisely control the structure, chemical, and physical properties of PBAs at the atomic level to achieve diverse redox reaction sites. In general, they can provide a high theoretical capacity of  $170 \text{ mAh g}^{-1}$ . In addition, PBAs have an open three-dimensional (3D) framework channel ( $4.6 \text{ \AA}$ ), which not only promotes the diffusion dynamics of protons but also reduces the lattice volume change caused by proton insertion/removal, showing excellent electrochemical reversibility and structural stability. Finally, PBAs electrode materials can be synthesized by chemical coprecipitation at room temperature and are

cheap to fabricate. Its low solubility exhibits excellent corrosion resistance to acid electrolytes. When the PBAs are synthesized by coprecipitation method, there are much vacancies and interstitial water molecules in the crystal structure, resulting in poor cycle life of PBAs metal ions-based carrier energy storage system. However, recent studies on PBAs-based proton storage have shown that the existences of interstitial water play an important role in proton transport. It is reasonable to design the PBAs containing zeolite  $H_2O$  or coordinated  $H_2O$  in the structure of PBAs for proton energy storage.

Taking hydrated CuPBAs with a large number of vacancies and interstitial water as an example in Fig. 3(b).<sup>37</sup> The CuPBAs material exhibited high-rate performance (providing a specific capacity of  $49 \text{ mAh g}^{-1}$  at  $4000 \text{ C}$ ) and ultralong cycle life (with a capacity retention rate of 60% after  $730\,000$  cycles at  $500 \text{ C}$ ), which is comparable to EDLCs. The mechanism could elucidate that the Grothuss proton

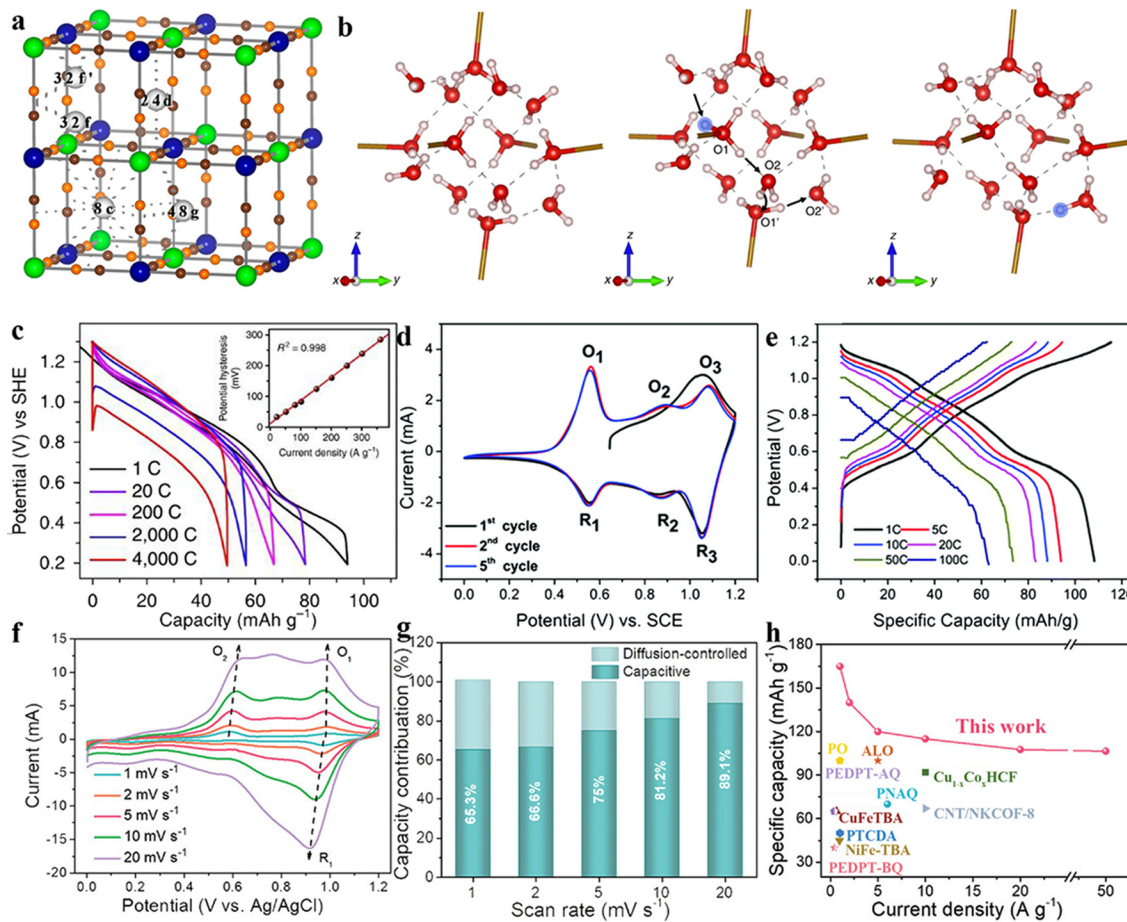
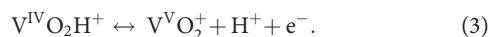
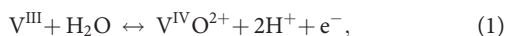


**FIG. 3.** Electrochemical performance and charge storage mechanisms of PBAs for proton storage. (a) Schematic illustration of the crystal structure of  $Fe_4[Fe(CN)_6]_3 \cdot 14H_2O$ . Reproduced with permission from Ling et al., J. Phys. Chem. C 117(41), 21158–21165 (2013). Copyright 2013 American Chemical Society.<sup>42</sup> (b) The DFT calculations transport path of protons and (c) GCD curves in CuPBAs. Reproduced with permission from Wu et al., Nat. Energy 4(2), 123–130 (2019). Copyright 2019 Springer Nature.<sup>37</sup> (d) CV curves ( $1.0 \text{ mV s}^{-1}$ ) and (e) GCD curves of VPBAs under different C-rates. Reproduced with permission from Peng et al., Chem. Commun. 56(79), 11803–11806 (2020). Copyright 2020 Royal Society of Chemistry.<sup>39</sup> (f) The CV curves, the capacitive, and (g) diffusion control contributions ratios at different scan rates and (h) the comparison of HVHCF electrode with other reported proton systems. Reproduced with permission from Dong et al., Adv. Funct. Mater. 33(11), 2210473 (2023). Copyright 2023 Wiley-VCH Verlag GmbH & Co. KGaA.<sup>41</sup>

migration can occur along a continuous hydrogen bonds network. Interestingly, the DFT calculations also proved the migration path of protons during the intercalation process, indicating that zeolite water is the optimal binding site for protons and demonstrates a low migration energy barrier of 0.15 eV. Therefore, utilizing the Grotthus proton mechanism to design the PBAs electrode materials provides a new approach for simultaneously obtain high-power density and high-energy density. Similar to the above work, the NiPBAs are further fabricated to achieve ultrahigh rate performance (6000 C), where the proton (de)insertion is capacitive behavior.<sup>38</sup> Despite the outstanding advantages of PBA in proton energy storage applications, the low capacities of CuPBAs (95 mAh g<sup>-1</sup>) and NiPBAs (65 mAh g<sup>-1</sup>) remain an unresolved issue. Recently, the VPBAs are prepared and delivered a high capacity of 108 mAh g<sup>-1</sup> by using the multi electron reaction of V elements, as depicted in Figs. 3(c)–3(e).<sup>39</sup> The high capacity of VHCF mainly derived from the two reversible redox of vanadium ( $V^{III} \leftrightarrow V^{IV} \leftrightarrow V^V$ ) and iron ( $Fe^{II} \leftrightarrow Fe^{III}$ ), which also contributed to the pseudocapacitive mechanism. However, compared with CuPBAs and NiPBAs, VPBAs exhibit poor rate performance and longer cycle life due to the lack of continuous hydrogen bonding networks.

To obtain complete and mobile protons during the preparation process, the pre-protonation is an effective strategy to prepare VPBAs or other PBAs electrode materials to maintain the excellent electrochemical performance. For instance, the pre-protonated  $H_xCu^{II}[Fe^{III}(CN)_6]_{2/3} \cdot 4H_2O$  electrode materials have a capacity of 95 mAh g<sup>-1</sup> at 2 A g<sup>-1</sup>.<sup>40</sup> However, the capacity and rate capability still cannot satisfy the demand for high energy/power requirement in the preliminary stage. Therefore, the pre-protonated VPBAs (HVPBAs) is prepared as the positive material to obtain satisfying capacity of proton-based electrodes [Figs. 3(f)–3(h)]. After pre-protonating HVPBAs provide the highest capacity to date of 155 mAh g<sup>-1</sup> at 1 A g<sup>-1</sup>.<sup>41</sup> Its capacitance still retains 80% of the initial capacity after 6000 cycles (10 A g<sup>-1</sup>), showing long cycling stability. Based on sufficient testing, the proton transport mechanism can be described as three steps



The establishment of hydrogen bond network significantly enhances the electrochemical performance of HVPBAs. This study not only provides a facile method to fabricate HVPBAs, but also promotes the prospect for the construction of promising proton-based device with high performance. In summary, it is an effective strategy for obtain high performance PBAs materials to construct a hydrogen bonding network and introduce multiple redox sites. Therefore, this research demonstrates that high-capacity PBAs nanoelectrode materials can be fabricated via various approaches, including different metal ion doping, nanostructure construction and further compounding with other materials.

### 3. Covalent organic frameworks

As electrode materials, the adjustable pore structure and rich redox-active groups of covalent organic frameworks (COFs), make

them a promising choice for proton transport. Moreover, the COFs with tunable structures can be prepared by facile methods. Since its first reported in 2013,<sup>43</sup> the COFs electrode materials have obtained widespread attention in the field of energy storage. In general, introducing the redox-active site is one of the efficient strategies to enhance the pseudocapacitive behavior of COFs. The most commonly used active sites are N and O groups. For example, a new COF of TDFFP-1 was fabricated and exhibited an excellent capacitance of 418 F g<sup>-1</sup> at 0.5 A g<sup>-1</sup> in H<sub>2</sub>SO<sub>4</sub> electrolytes [Fig. 4(a)].<sup>44</sup> The excellent reversible reaction is attributed to the protonation of the imine bond. Subsequently, a novel 3D COF electrode material with a pyridinyl radical was synthesized.<sup>45</sup> The energy storage mechanism can be described as a pyridine ring system reversibly taking one H<sup>+</sup> and one e<sup>-</sup>. In addition to introducing redox-active sites into COFs, other new strategies, such as generating charge transfer, enhancing proton, and electronic conduction, have also been demonstrated to create novel COFs with enhanced pseudocapacitance. For instance, two COFs, namely, TpPa-(OH)<sub>2</sub> and TpBD-(OH)<sub>2</sub>, have been successfully synthesized via the Schiff-base condensation route, as demonstrated in Figs. 4(b)–4(d).<sup>46</sup> The reversible proton-coupled electron transfer derived from hydroquinone/benzoquinone (H<sub>2</sub>Q/Q) moieties of TpPa-(OH)<sub>2</sub> delivers a high capacitance of 416 F g<sup>-1</sup> at 0.5 A g<sup>-1</sup>. After 1000 cycles, the specific capacitance of COF electrodes still maintains 66% capacitance of that initial value at a current density of 5 A g<sup>-1</sup>. The good pseudocapacitive behavior can be attributed to 2H<sup>+</sup>/2e<sup>-</sup> proton-coupled electron transfer, which belongs to the reaction of the H<sub>2</sub>Q/Q redox transition. This work provides a notable way to design efficient proton-based pseudocapacitors. In addition, to simultaneously achieve high energy density and power density, two novel COFs (NKCOF-8 and NKCOF-2) with N=N groups and azo groups were first fabricated by using the Grotthus proton-conductive mechanism [Figs. 4(e)–4(g)].<sup>47</sup> After combined with carbon nanotubes, the composites deliver an unprecedented high capacitance of 440 F g<sup>-1</sup> at 0.5 A g<sup>-1</sup>, exceeding most COFs-based supercapacitors. After 10000 cycles, the capacitance remains at 90% of the initial capacitance. Obviously, COFs are a promising new class of materials for proton storage. Although extensive efforts have been explored to enhance the proton storage capabilities of COFs-based supercapacitors, achieving practical applications remains a huge challenge.

### 4. Miscellaneous materials

Electrode materials play a crucial role in the performance of proton supercapacitors. In addition to the above-mentioned positive electrode materials, other miscellaneous materials or composites have also been designed as promising candidates for proton storage. Recently, ruthenium dioxide (RuO<sub>2</sub>) has been utilized in proton supercapacitors.<sup>48</sup> It can be concluded that RuO<sub>2</sub> delivers a faster H<sup>+</sup> transportation by the pathway of the [001] direction than the [110] direction due to the lower charge barrier. This study can provide inspiration and new ideas for electrode material preparation. In addition, tannins, as the renewable materials, are extracted and used as positive electrode materials for the first time. When comminuted with the conductive polypyrrole (PPy), this hybrid electrode materials exhibit a remarkable capacitance of 370 F g<sup>-1</sup> at 0.5 A g<sup>-1</sup>.<sup>49</sup> The proton charge storage mechanism is attributed to the phenolic groups in tannins, and it can occur a redox reaction involving two protons and two electrons. Similarly, the PPy/Cu coordination polymer composite material

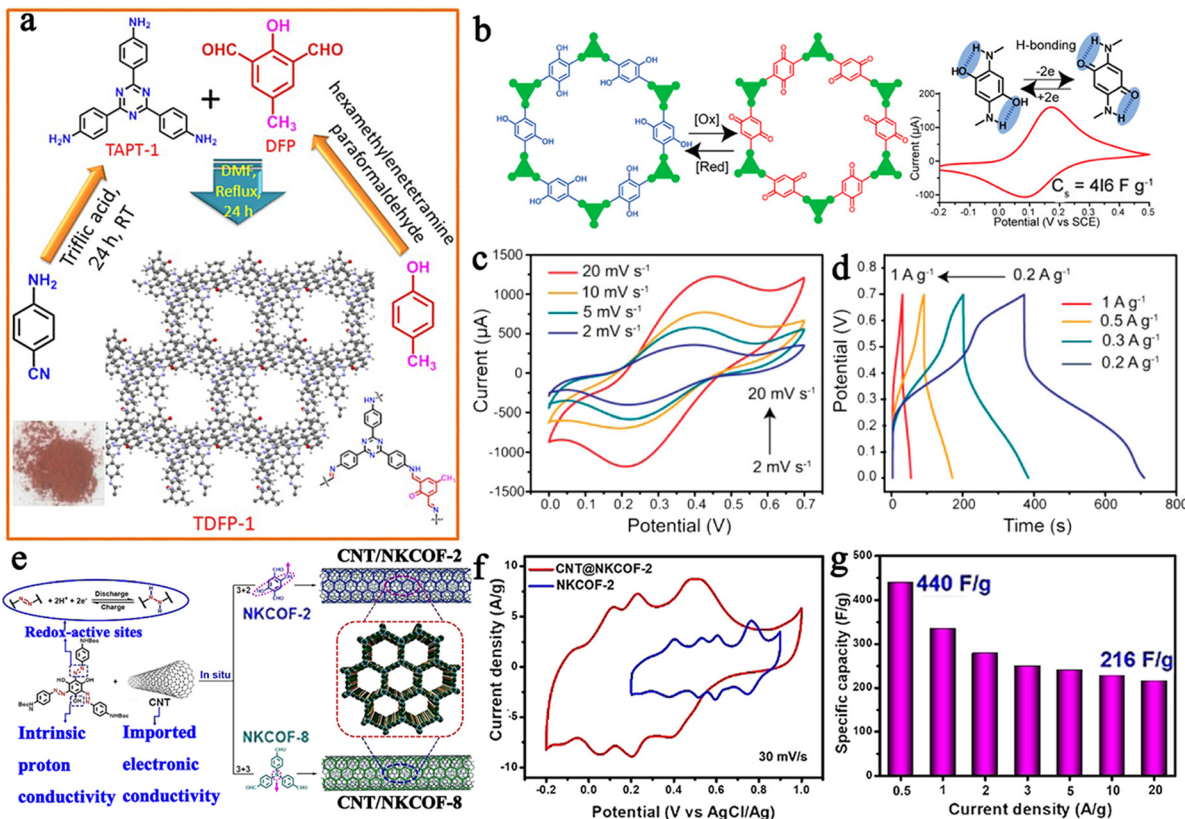


**FIG. 4.** Electrochemical performance and charge storage mechanisms of COFs for proton storage. (a) The fabrication process of TDFP-1 COF. Reproduced with permission from Bhajna *et al.*, ChemSusChem. **10**(5), 921–929 (2017). Copyright 2017 Wiley-VCH Verlag GmbH & Co. KGaA. (b) The synthesis illustration, (c) CV, and (d) GCD curves of TPpa-(OH)<sub>2</sub>, respectively. Reproduced with permission from Chandra *et al.*, Chem. Mater. **29**(5), 2074–2080 (2017). Copyright 2017 American Chemical Society.<sup>46</sup> (e) The synthesis scheme of CNT/NKCOF-2 and CNT/NKCOF-8, (f) CV curves and (g) specific capacity of CNT/NKCOF-2. Reproduced with permission from Yang *et al.*, Angew. Chem., Int. Ed. **60**(40), 21838–21845 (2021). Copyright 2021 Wiley-VCH Verlag GmbH & Co. KGaA.<sup>47</sup>

achieved a high specific capacitance ( $\sim 500 \text{ F g}^{-1}$ ) and potential window (0.8 V) in 0.5 M H<sub>2</sub>SO<sub>4</sub> electrolytes.<sup>50</sup> In conclusion, designing positive electrode materials that offer a wide potential window is essential, as usually only PBA is selected as the most promising candidate.

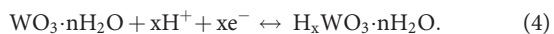
## B. Negative electrode materials

### 1. Tungsten oxides

Tungsten oxides (WO<sub>3-x</sub>) have emerged as promising negative electrode materials for pseudocapacitor applications due to their superior characteristics, including high electrical conductivity ( $10^{-6}$ – $10 \text{ S cm}^{-1}$ ), abundant oxidation states (W<sup>2+</sup>–W<sup>6+</sup>), low cost, and excellent electrochemical stability.<sup>51</sup> The hexagonal WO<sub>3</sub> (*h*-WO<sub>3</sub>) with a six-membered-ring tunnel structure can store the H<sup>+</sup> to achieve fast intercalation pseudocapacitance [Fig. 5(a)]. Although the *h*-WO<sub>3</sub> was first discovered as early as in 1979, the *h*-WO<sub>3</sub> used in proton-based supercapacitors only began to attract the researchers' attention until 2014.<sup>52–54</sup> The *h*-WO<sub>3</sub> with a nanopillar structure was synthesized and used for the first time as a proton-insertion electrode, showing a higher specific capacitance of 421.8 F g<sup>-1</sup> (0.5 A g<sup>-1</sup>) than that of previous studies.<sup>55</sup> The *h*-WO<sub>3</sub> possesses large space tunnels (0.49 nm) in the

[100] direction, which are five times larger than that of tetragonal tunnels and benefit for deeper proton intercalation. However, the proton intercalation mechanism still requires to be further elucidated. Then, an *h*-WO<sub>3</sub> electrode is prepared and delivered a significantly high volumetric capacitance value of  $\sim 2000 \text{ F cm}^{-3}$ , which is attributed to the crystalline water in the tunnel structure of *h*-WO<sub>3</sub> [Figs. 5(b) and 5(c)].<sup>56</sup> Unfortunately, the charge storage mechanism involving the H<sup>+</sup> insertion process in WO<sub>3</sub> remains unclear so far.

In addition to *h*-WO<sub>3</sub>, the researcher first elucidated the structural water of WO<sub>3</sub> enable to promote the proton-insertion process via the Grothuss transport mechanism until 2018. A WO<sub>3</sub>·0.6H<sub>2</sub>O electrode was prepared, and then its proton mechanism is investigated by utilizing EQCM.<sup>27,57</sup> During the first protonation process, WO<sub>3</sub> deserted and inserted about 0.25 lattice H<sub>2</sub>O stimulatingly (0–0.25 V). Then  $\sim 0.30$  naked proton was incorporated (−0.25 to −0.40 V), followed by  $\sim 0.17$  H<sub>3</sub>O<sup>+</sup> inserted afterward (−0.40 to −0.55 V). Therefore, the proton storage process of WO<sub>3</sub> can be described as follows:



The insertion or desorption of protons are reversible pseudocapacitive kinetics, showing promising rate performance and long cycle life

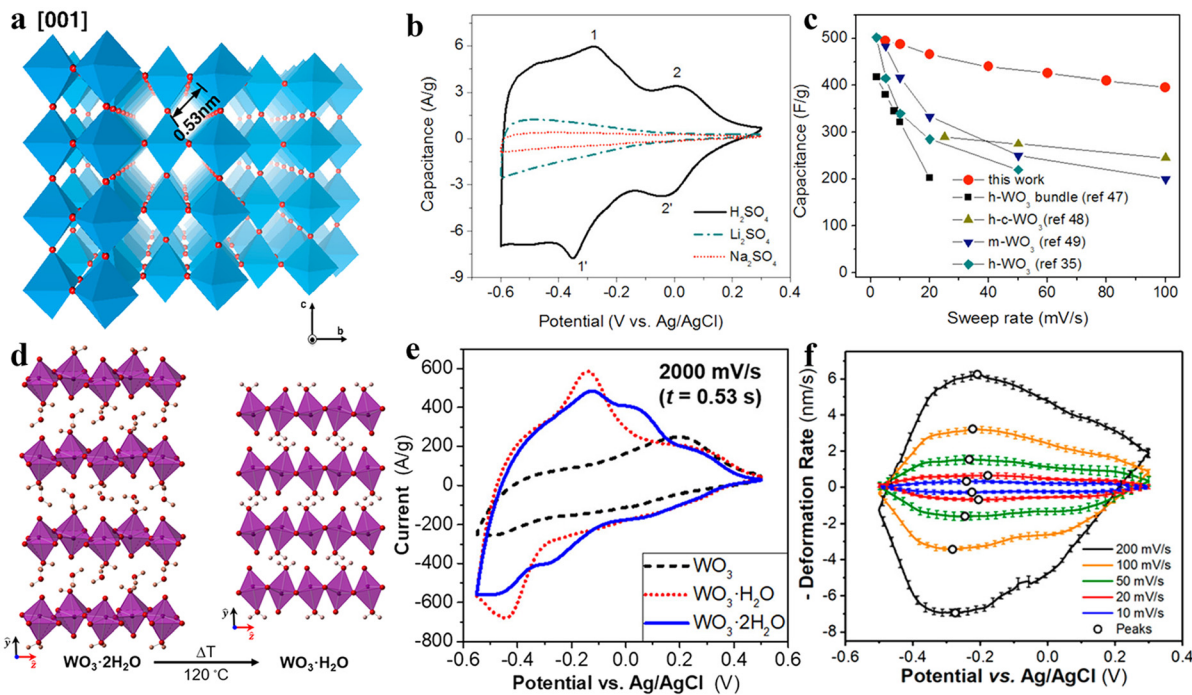


**FIG. 5.** Crystal structures and electrochemical performance of tungsten oxides for proton storage. (a) Schemes of *h*-WO<sub>3</sub> crystal structure along the [001] directions. Reproduced with permission from Zhu *et al.*, ACS Appl. Mater. Interfaces **6**(21), 18901–18910 (2014). Copyright 2014 American Chemical Society.<sup>61</sup> (b) CV curves of *h*-WO<sub>3</sub>·nH<sub>2</sub>O electrodes in H<sub>2</sub>SO<sub>4</sub>, Li<sub>2</sub>SO<sub>4</sub>, and Na<sub>2</sub>SO<sub>4</sub> electrolytes, respectively and (c) Comparison of capacitance of *h*-WO<sub>3</sub>·nH<sub>2</sub>O with other WO<sub>3</sub> electrodes. Reproduced with permission from Chen *et al.*, Nano Lett. **15**(10), 6802–6808 (2015). Copyright 2015 American Chemical Society.<sup>56</sup> (d) The crystal structures of WO<sub>3</sub>·2H<sub>2</sub>O and WO<sub>3</sub>·H<sub>2</sub>O. (e) The CV curves of WO<sub>3</sub> electrodes in 0.5 M H<sub>2</sub>SO<sub>4</sub> at 2 V s<sup>-1</sup>. Reproduced with permission from Mitchell *et al.*, ACS Energy Lett. **4**, 2805–2812 (2019). Copyright 2019 American Chemical Society.<sup>50</sup> (f) The relationship between deformation rate and potential at sweep rates of WO<sub>3</sub>·2H<sub>2</sub>O. Reproduced with permission from Wang *et al.*, ACS Nano **12**(6), 6032–6039 (2018). Copyright 2018 American Chemical Society.<sup>59</sup>

(20 000 cycles). Then, it is an important concern that whether the presence of lattice water in WO<sub>3</sub> is key for proton storage. The WO<sub>3</sub>·2H<sub>2</sub>O electrode materials possess layered crystal structure, and its interlayer spacing is larger than the crystal tunnel of *h*-WO<sub>3</sub>. Interestingly, the energy storage mechanism of WO<sub>3</sub>·2H<sub>2</sub>O is also a pseudocapacitive process. For instance, WO<sub>3</sub>·2H<sub>2</sub>O demonstrated an outstanding areal capacitance of 0.25 F cm<sup>-2</sup> for proton storage at a fast scan rate of 200 mV s<sup>-1</sup>.<sup>58</sup> It is noteworthy that the rate capability of WO<sub>3</sub>·2H<sub>2</sub>O approaches nearly 100%, which can be attributed to its hydrated structure. Then, Augustyn's group has clearly explained the surface-limited mechanism of WO<sub>3</sub>·2H<sub>2</sub>O by using operando atomic force microscopy and *ex situ* XRD test, as shown in Figs. 5(d)–5(f). These results imply that fabricate layered electrode materials with confined structural water is an effective strategy to achieve high-rate capabilities in proton ion storage.

## 2. Molybdenum oxides

Molybdenum oxides (MoO<sub>x</sub>), especially crystalline MoO<sub>3</sub>, are regarded as a promising proton electrode material because of its stable layered structure, large potential widow, and high valence state of the Mo element.<sup>62</sup> In general, the typical layered MoO<sub>3</sub> can be formed by Mo unit sharing sides or corners, as depicted in Fig. 6(a). Hence, MoO<sub>3</sub> has been widely used in proton energy storage due to its wide

interlayer space for proton intercalation.<sup>63</sup> In 2018, Wang and his group first identified the proton intercalation process in MoO<sub>3</sub> and delivered a high capacity of 88 mAh g<sup>-1</sup> at 100 C.<sup>64</sup> The above work also confirmed that the proton intercalation process is fully reversible in the range of -0.2 to 0.3 V, while the irreversible process occurred in the range of -0.2 to 0.5 V according to Faraday's law. Until 2020, the proton-insertion mechanism of MoO<sub>3</sub> was elucidated via advanced *in situ* characterization, which subsequently attracted widespread attention. The MoO<sub>3</sub> electrode achieved a high areal capacity of 22.4 mAh cm<sup>-2</sup>, which is attributed to the fast proton Grotthuss's mechanism [Figs. 6(b)–6(d)].<sup>29</sup> The detailed reaction that occurred can be described and identified by *in situ* characterization techniques as follows:



At first discharge (-0.5 V), the high-content (2.0 mol) H<sup>+</sup> is intercalated into MoO<sub>3</sub> to fabrication of H<sub>2</sub>MoO<sub>3</sub>. Then, the 0.9 mol H<sup>+</sup> first filled the intralayer sites of oxygen atoms of the Mo<sub>6</sub> octahedra. The subsequent 1.1 mol H<sup>+</sup> occupied the interlayer positions and act as charge carriers. Therefore, the 1.1 mol H<sup>+</sup> can be reversibly inserted into the electrode (0.3 V). Additionally, the *in situ* XRD of MoO<sub>3</sub> was furthered emphasized these two-phase reactions during

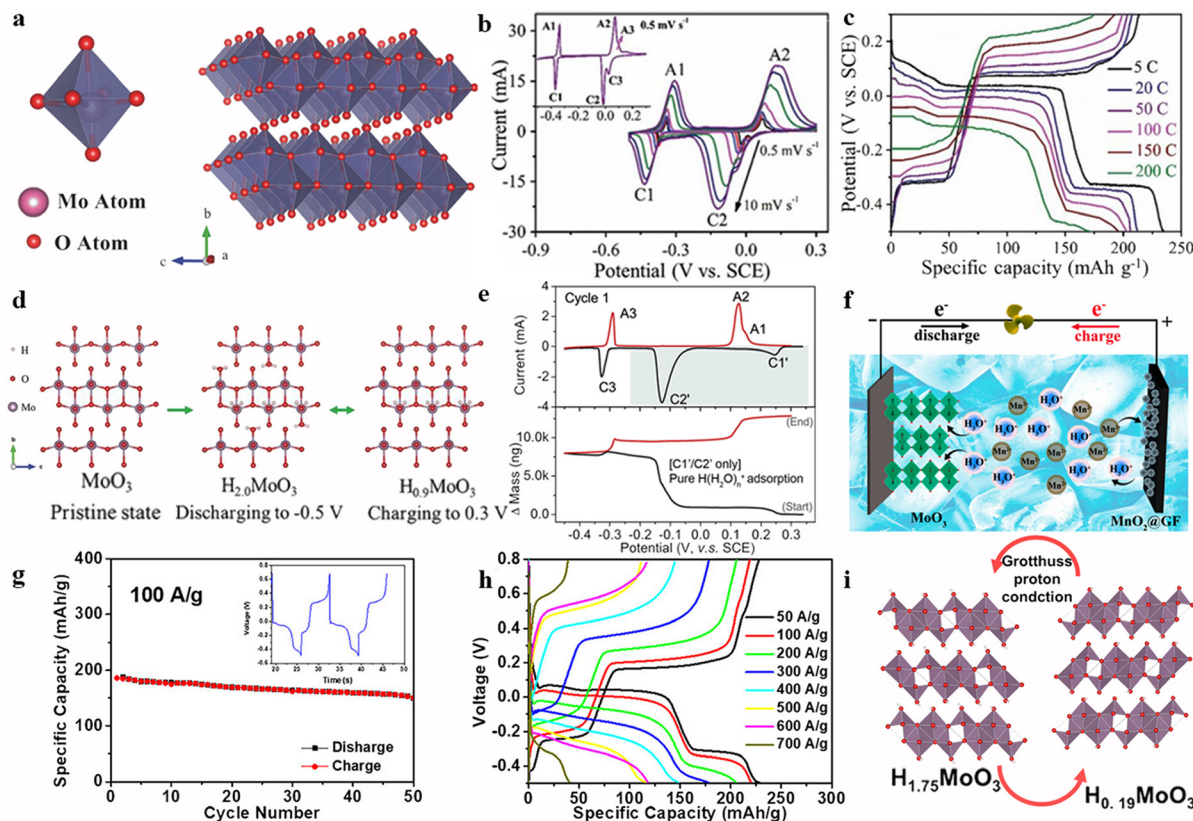


**FIG. 6.** Electrochemical performance and charge storage mechanisms of molybdenum oxides for proton storage. (a) The lattice structure of  $\alpha$ -MoO<sub>3</sub>. Reproduced with permission from de Castro *et al.*, *Adv. Mater.* **29**(40), 1701619 (2017). Copyright 2017 Wiley-VCH Verlag GmbH & Co. KGaA.<sup>62</sup> (b) The CV and (c) GCD curves in the H<sub>2</sub>SO<sub>4</sub> electrolyte, and (d) the schematic of proton insertion mechanism during the cycling of the MoO<sub>3</sub> electrode. Reproduced with permission from Su *et al.*, *Adv. Funct. Mater.* **30**(46), 2005477 (2020). Copyright 2020 Wiley-VCH Verlag GmbH & Co. KGaA.<sup>29</sup> (e) The first CV and electrochemical quartz crystal microbalance curves, and (f) proton energy storage application of MoO<sub>3</sub> electrode. Reproduced with permission from Guo *et al.*, *Cell Rep. Phys. Sci.* **1**(10), 100225 (2020). Copyright 2020 Elsevier.<sup>65</sup> and Reproduced with permission from Yan *et al.*, *ACS Energy Lett.* **5**(2), 685–691 (2020). Copyright 2020 American Chemical Society.<sup>66</sup> (g) The cycling performance at 100 A g<sup>-1</sup>, (h) GCD curves, and (i) schematic illustration of the Grothuss proton process of H<sub>1.75</sub>MoO<sub>3</sub> electrodes. Reproduced with permission from Xu *et al.*, *J. Am. Chem. Soc.* **144**(38), 17407–17415 (2022). Copyright 2022 American Chemical Society.

24 October 2024 08:41:11

cycling as shown in Fig. 6(e).<sup>65</sup> The above result has also been confirmed by another group [Fig. 6(f)].<sup>66</sup>

Although  $\alpha$ -MoO<sub>3</sub> achieves excellent electrochemical performance in proton energy storage, poor conductivity and diffusion-limited kinetics still hinder its widespread application. Therefore, to improve the proton diffusion kinetics, researchers have explored various strategies, including extending layer spacing by H<sup>+</sup> interstitial doping and introducing oxygen vacancies.<sup>67,68</sup> For instance, metallic H<sub>1.75</sub>MoO<sub>3</sub> nanobelts have been successfully fabricated, showing a high capacity of 111 mAh g<sup>-1</sup> at 200 mA g<sup>-1</sup>, which is superior to previously reported proton insertion electrodes [Figs. 6(g) and 6(h)].<sup>69</sup> It is important to highlight that the energy storage mechanism of H<sub>1.75</sub>MoO<sub>3</sub> nanobelts is capacitive-limited behavior, dominated by the Grothuss proton process, which paves the way for proton energy storage systems. Furthermore, a MoO<sub>3</sub>/PANI composite electrode was prepared by oxygen vacancy engineering and demonstrated a high capacitance of 1307.4 F g<sup>-1</sup> at a current density of 1 A g<sup>-1</sup>.<sup>70</sup> This work also evaluated the electrochemical performance of MoO<sub>3</sub>/PANI in various electrolytes, including H<sub>2</sub>SO<sub>4</sub>, Na<sub>2</sub>SO<sub>4</sub>, and Li<sub>2</sub>SO<sub>4</sub>. The

capacitance of MoO<sub>3</sub> in the H<sub>2</sub>SO<sub>4</sub> electrolyte is highest, indicating that the larger Li<sup>+</sup> and Na<sup>+</sup> face challenges during insertion. Interestingly, MoO<sub>3</sub> is also capable of facilitating fast proton insertion in other metal ions-based batteries, such as Al, Li, and Zn, which broadens its applicability in energy storage systems.<sup>21,71,72</sup>

### 3. Vanadium oxides

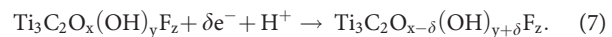
As a class of traditional functional material, vanadium oxides are (V<sub>2</sub>O<sub>5</sub>, VO<sub>x</sub>) regarded as a promising electrode material owing to their advantage of multiple oxidation states, low cost, wide resources, etc. In addition, one of the primary charge storage mechanisms of VO<sub>x</sub> has been investigated as the reversible H<sup>+</sup> (de)intercalation mechanism. For example, as depicted in Figs. 7(a)–7(c), the fabricated Al/V<sub>2</sub>O<sub>5</sub> based device demonstrates that H<sup>+</sup> is first inserted into the V<sub>2</sub>O<sub>5</sub> electrode rather than other metal ions in an acid electrolyte, achieving a high capacity of 200 mAh g<sup>-1</sup>.<sup>73</sup> The main reason can be explained as the reversible reaction between V<sub>2</sub>O<sub>4</sub> and H<sub>1.43</sub>V<sub>2</sub>O<sub>5</sub> by using the XRD test. Recently, Chen and his group prepared the VO<sub>x</sub> electrode with a

large interlayer distance of 1.15 nm, which facilitates the co-insertion of  $H^+$  and  $Zn^{2+}$  [Fig. 7(d)].<sup>74</sup> Hence, both  $H^+$  and  $Zn^{2+}$  play a role in the charge storage processes. Thus, the electrolyte engineering strategies (e.g., pH regulation,  $Zn^{2+}$  concentration control, etc) have been proven to provide an efficient method in preparing  $VO_x$ -based positive electrodes, as demonstrated in Figs. 7(e) and 7(f). Since then, the co-insertion mechanism of  $Zn^{2+}$  and  $H^+$  has gradually attracted the attention of researchers. Although many studies have confirmed the existence of proton insertion in vanadium oxides, a deep understanding and detailed characterization of proton insertion is still lacking. In the future, it is highly desired to exploit new cognition for vanadium oxides material design or utilize proton intercalation mechanism to obtain high energy density and long cycle stability materials.

#### 4. MXenes

MXenes, a new type of two-dimensional layered crystal material, are first discovered in 2011 by Gogotsi's research group. They are typically prepared through selective etching the Al layer of  $Ti_3AlC_2$  using HF.<sup>75</sup> The named "MXene" is used to emphasize its graphene-like two-dimensional material properties, as depicted in Fig. 8(a). MXenes have outstanding pseudocapacitive performance for proton storage because of their excellent electrical conductivity, large two-dimensional structure, and abundant surface-active sites.<sup>76</sup> It is noteworthy that the MXenes have delivered the highest volumetric capacitance of  $1500 \text{ F cm}^{-3}$  and long cycling stability of over 10 000 cycles in the  $H_2SO_4$  electrolyte (within a potential window of  $-0.8$  to  $0.2 \text{ V}$ ), which is comparable to the unparalleled capabilities of  $RuO_2$  [Fig. 8(b)].<sup>19</sup> Additionally, Gogotsi and Simon's group believed that the high capacitance was generated from the proton intercalation pseudocapacitance.

To prove this hypothesis, x-ray absorption spectroscopy was used to monitor changes of Ti oxidation state. They observed that the oxidation state of Ti shifted from 2.33 to 2.46 as the potential varied from 0.275 to  $-0.35 \text{ V}$  [Figs. 8(c) and 8(d)].<sup>77</sup> Therefore, the pseudocapacitance of  $Ti_3C_2T_x$  is contributed to the changes in the Ti oxidation state. The proposed reaction mechanism for rapid storage of  $H^+$  in  $Ti_3C_2T_x$  has been proved as follows:



Additionally, to thoroughly understand the mechanism of MXene in proton intercalation, the *in situ* XRD test and DFT calculation were employed to analysis changes in c-lattice parameter of MXene.<sup>78</sup> The XRD was performed at 2 theta degree range of 5–20. The hypothesis on energy storage mechanism of  $H^+$  in  $Ti_3C_2T_x$  can be proved that (1) the lattice of MXene can shrink by  $0.1 \text{ \AA}$  from 0 to  $-0.6 \text{ V}$ , belonging to  $H^+$  intercalation. (2) Below  $-0.6 \text{ V}$ , the lattice expands by  $0.5 \text{ \AA}$ , whereas  $Ti_3C_2$  with OH-termination expanded. These results are the first to demonstrate changes in c-lattice parameter of MXene and confirm pseudocapacitive mechanism for proton storage, which accounts for observed high capacitance performance.

Although considerable studies have deeply clarified the charge storage mechanisms of proton insertion into the MXenes layers in acidic electrolytes, the role of confined water within the MXenes layers and its impact on pseudocapacitive behavior still need to be investigated. Wang *et al.* demonstrated that the content of  $-O$  functional groups and the presence of more interlayer water in MXenes can highly enhance the capacitance.<sup>79</sup> For instance, by regulating the content of  $-O$  functional group to 2, MXenes showed an ultrahigh capacitance of  $1190 \text{ F g}^{-1}$  ( $167 \text{ F g}^{-1}$  upon the content of  $-O$  functional group is 0.28), which is nearly the theoretical capacitance. The

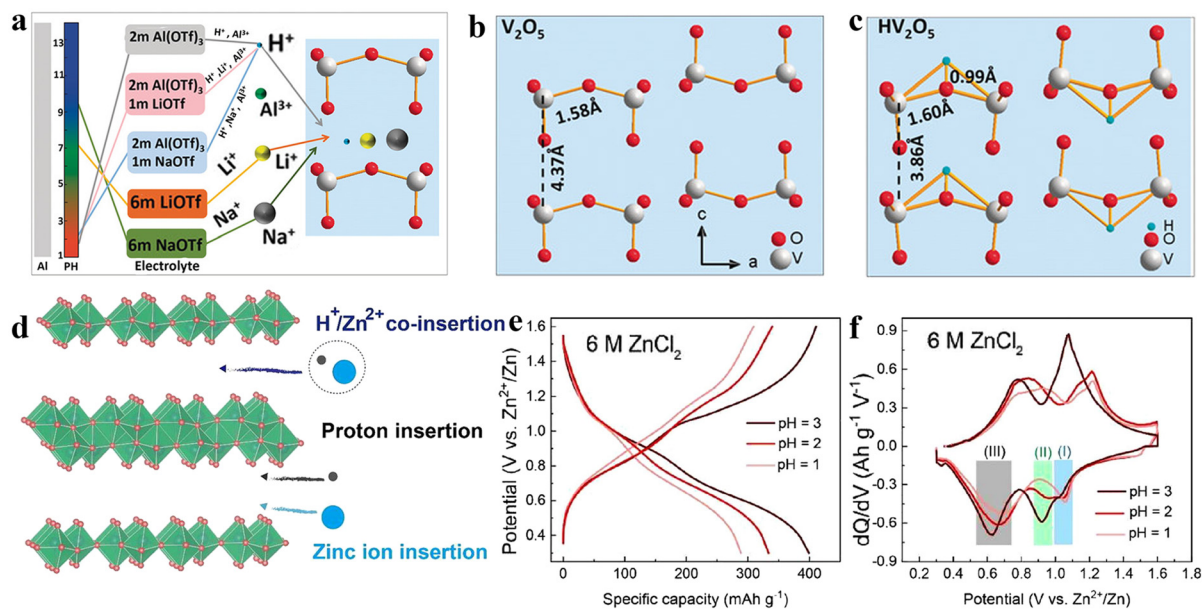


**FIG. 7.** Electrochemical performance and charge storage mechanisms of vanadium oxides for proton storage. (a) The ions intercalation/de-intercalation principles of  $V_2O_5$  in aqueous Al cells. Structure illustration of (b)  $V_2O_5$  and (c)  $HV_2O_5$ . Reproduced with permission from Zhao *et al.*, Angew. Chem., Int. Ed. 59(8), 3048–3052 (2020). Copyright 2020 American Chemical Society.<sup>73</sup> (d) The schematical illustration of  $H^+/Zn^{2+}$  co-insertion in  $VO_x$  materials. (e) The GCD and (f) CV curves of  $VO_x$  in different  $ZnCl_2$  electrolytes through regulating the pH. Reproduced with permission from Pan *et al.*, Chem. Eng. J. 419, 129491 (2021). Copyright 2021 Elsevier.<sup>74</sup>

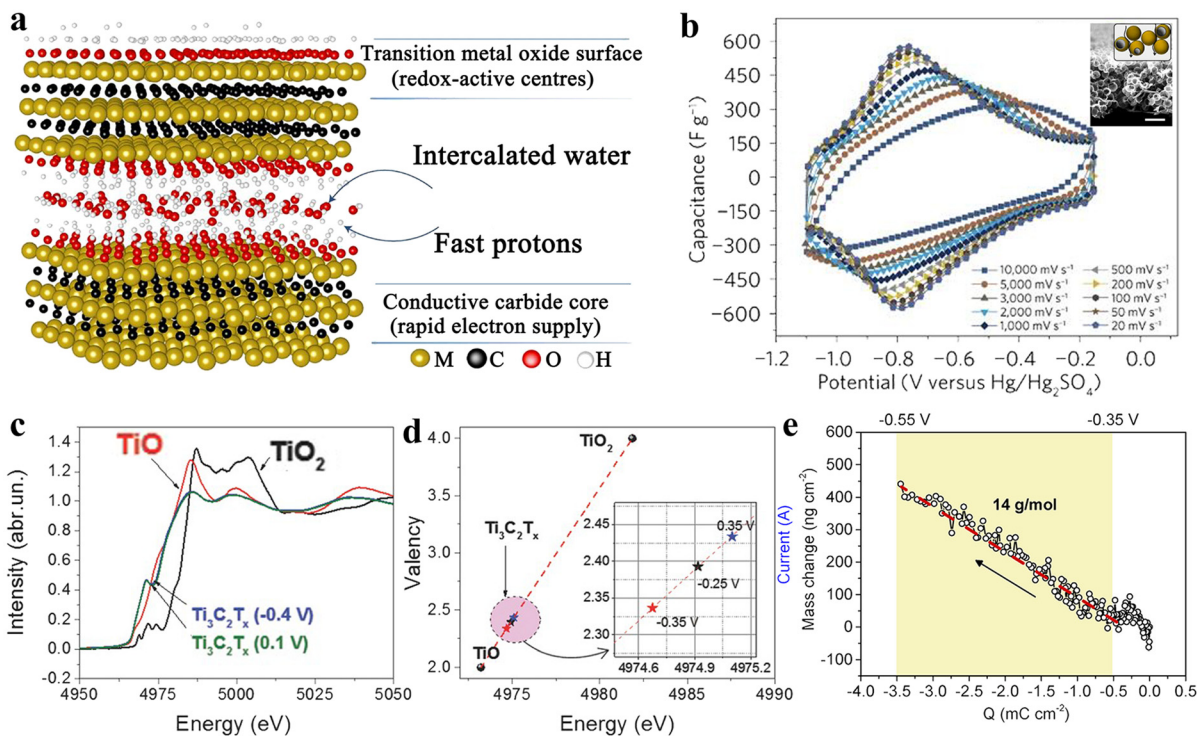


**FIG. 8.** Electrochemical performance and characterizations of MXenes based electrodes for proton storage. (a) Schematic structure of MXene and (b) CV curves at 10–100 000 mV s<sup>-1</sup> of MXene electrode. Reproduced with permission from Lukatskaya *et al.*, Nat. Energy, **2**(8), 17105 (2017). Copyright 2017 Springer Nature.<sup>19</sup> (c) The Ti K-edge XANES spectra of  $\text{Ti}_3\text{C}_2\text{T}_x$ ,  $\text{TiO}$ , and  $\text{TiO}_2$ , respectively, and (d) the average Ti oxidation state of  $\text{Ti}_3\text{C}_2\text{T}_x$  at various potentials. Reproduced with permission from Lukatskaya *et al.*, Adv. Energy Mater. **5**(15), 1500589 (2015). Copyright 2015 Wiley-VCH Verlag GmbH & Co. KGaA.<sup>77</sup> (e) The mass change vs charge of P-MXene electrode. Reproduced with permission from Shao *et al.*, ACS Energy Lett. **5**(9), 2873–2880 (2020). Copyright 2020 American Chemical Society.<sup>82</sup>

24 October 2024 0:8:41:11

interlayer water in MXenes plays a vital role for enhancing pseudocapacitance; however, it still lacks a deep understanding mechanism between the proton transfer and MXene layers. Several studies have proved that the proton transfer can be improved with an increasing number of water-layers and it follows the Eigen-Zundel-Eigen mechanism.<sup>80,81</sup> For example, the proton storage mechanism in MXenes was unraveled by *in situ* testing and molecular dynamics (MD) simulations, as shown in Fig. 8(e).<sup>82</sup> These findings confirmed that  $\text{H}_2\text{O}$  confined between MXene layers can trigger the redox activity of Ti, enabling fast charge compensation through the high diffusion rate of protons via the Grotthus mechanism. This study offers an effective strategy to obtain high-performance MXenes electrodes. Recently, researcher conducted a nanoscale electrochemical measurement on monolayer  $\text{Ti}_3\text{C}_2\text{T}_x$  over a small subregion of  $0.3 \mu\text{m}^2$  to observe the pseudocapacitive charging response.<sup>83</sup> It can be concluded that the specific gravimetric capacitance of MXene is independent of the flake size, and the proton transport of MXene is ultrafast ( $>1000 \text{ V s}^{-1}$ ), demonstrating that the entire MXene flake is very active in generating proton pseudocapacitance.

## 5. Other materials

In addition to the electrode materials summarized above, other promising negative electrode materials have also been proposed in

recent years such as metal selenides and carbon composites. For instance, oxygen incorporated  $\text{MoSe}_2$  ( $\text{O}-\text{MoSe}_2$ ) has been fabricated as a host negative material for proton storage.<sup>84</sup> It was found that this layered  $\text{O}-\text{MoSe}_2$  exhibits high electronegativity, which is benefit to the binding of  $\text{H}^+$ . As a result,  $\text{O}-\text{MoSe}_2$  delivered a higher pseudocapacity of  $258 \text{ mAh g}^{-1}$  than pure  $\text{MoSe}_2$  of  $106 \text{ mAh g}^{-1}$  at a current density of  $0.1 \text{ A g}^{-1}$ . Following a similar design idea, researchers successfully synthesized a molybdenum phosphate (MP) electrode via introduction of  $\text{PO}_4^{3-}$  into  $\text{MoO}_x$ .<sup>85</sup> The MP materials with high electronegativity show novel proton intercalation in mild electrolytes, which well solves the corrosion issues for electrode materials and current collectors in proton energy storage. How to obtain electrode with excellent mechanical roughness is a major challenge for flexible proton supercapacitors. The COFs/MXene flexible composite (CMFs) materials have been constructed as a promising negative electrode material, providing a high specific capacitance of  $390 \text{ F g}^{-1}$  at  $0.5 \text{ A g}^{-1}$ .<sup>86</sup> After assembling the proton supercapacitor based on CMFs and carbon aerogel, the device displays a high potential window of  $1.4 \text{ V}$ , a maximum energy density of  $27.5 \text{ Wh Kg}^{-1}$ , and long cycling stability of over 20 000 cycles. This research provides a new strategy for fabricating flexible proton supercapacitors. Despite significant progress in negative electrode materials for proton storage, challenges such as short cycle life and dissolution in acidic electrolytes limit their further development. Overall, the fabrication of low-cost, high-energy density,

safe, and stable electrode materials is conducive for the future practical application of proton supercapacitors.

#### IV. PROTON STORAGE BASED FLEXIBLE SUPERCAPACITORS

With the rapid growth demand for flexible energy storage devices, flexible supercapacitors have gained widespread attention in wearable and portable electronics applications.<sup>87,88</sup> Compared to lithium-ions batteries, these devices are particularly appealing due to their safety, lightweight, long cycling life, superior flexible, and high-power density. However, it is well known that simultaneously improving the energy density and power density of flexible supercapacitors remains a challenge. Employing proton storage strategy has been recognized as an effective way to break the traditional limitations of supercapacitors, enabling enhanced capacitance and faster electrochemical kinetics. We comprehensively review the remarkable electrochemical performance of electrode materials developed in recent years. We will highly discuss the latest advancements in the design and practical applications of flexible proton-based flexible supercapacitors, with a particular emphasis on their integration into portable or wearable devices. Furthermore, we will provide an overview of current challenges and future prospect of proton-based flexible supercapacitors, especially in the internet of everything (IoE) applications.

Flexible supercapacitors are typically divided into symmetric and asymmetric supercapacitors based on the similarity of materials used for the positive and negative electrode. Considering the increased potential window and energy density, the manufacture of asymmetric supercapacitors is an efficient way. For instance, an all-asymmetric flexible supercapacitor with a wide potential window of 1.5 V has been developed, as shown in Figs. 9(a)–9(c).<sup>89</sup> The positive and negative electrodes are RuO<sub>2</sub> and MXene, respectively. Notably, this device exhibits a high energy density of 37  $\mu\text{W h cm}^{-2}$  and a long cycle life of over 20 000 cycles, which is benefit for the proton-induced pseudocapacitance. However, the high cost of RuO<sub>2</sub> limits its widespread applications. The high-energy density proton-based supercapacitors are further developed by using carbon nanotubes and MXenes materials.<sup>90</sup> This device offers a high energy density of 62 Wh Kg<sup>-1</sup> and a wide potential window of 1.6 V [Fig. 9(d)], which is superior to MXenes based supercapacitors. Furthermore, the two integrated supercapacitors can stable power a set of LEDs, as shown in Figs. 9(e) and 9(f). To further improve the energy density of the proton-based flexible supercapacitors, a new asymmetric supercapacitor is fabricated by using the CuCoPBAs and WO<sub>3</sub>·nH<sub>2</sub>O. This supercapacitor not only deliver ultrahigh energy density of 35 Wh kg<sup>-1</sup> but also has a wide window potential of 1.7 V.<sup>91</sup> The excellent electrochemical performance of CuCoPBAs in acid aqueous electrolytes opened new scene for preparing positive electrode that can suffer from the corrosiveness of acid electrolytes. To satisfy the demand for wearable electronics, a flexible supercapacitor has been manufactured on fabric substrate by employing MoO<sub>3-x</sub>/WO<sub>3-x</sub> as the negative electrode. This device provides a wide potential window of 1.9 V, a high capacitance of 216 mF cm<sup>-2</sup>, and a long cycle stability of 10 000 cycles.<sup>92</sup> Despite its excellent electrochemical performance, the supercapacitor's light weight, flexibility, and wearability make it a promising candidate for flexible electronics. Recently, it is a challenge to construct the flexible supercapacitors through scalable and low-cost fabrication process. For instance, a proton-based flexible supercapacitor has been prepared via lithography

by using CuFePBA as the positive electrode and Ti<sub>3</sub>C<sub>2</sub>T<sub>x</sub> as the negative electrode, as depicted in Fig. 9(g).<sup>93</sup> In particular, the device shows a wide potential window of 1.6 V, a high areal capacitance of 198 mF cm<sup>-2</sup>, and an excellent energy density of 70.5  $\mu\text{Wh cm}^{-2}$  (at a power density of 0.74 mW cm<sup>-2</sup>) [Figs. 9(h) and 9(i)]. This outstanding work provides new prospects for large-scale production of proton-based flexible supercapacitors.

Many developments of proton-based flexible supercapacitors have been achieved, such as enlarging the potential window by designing asymmetric electrode structures, using fabric substrates to satisfy the wearable demands, and providing the strategy for low-cost manufacture platform. However, the applications of proton flexible supercapacitors in harsh conditions, such as polar, aerospace, and military, are still restricted by low mass loading (<2 mg cm<sup>-2</sup>) and the freezing of the electrolytes at low-temperature. Therefore, a 3D-printed proton supercapacitor has been developed by utilizing PBAs and WO<sub>3</sub> as positive and negative electrodes, respectively, as depicted in Figs. 10(a) and 10(b).<sup>94</sup> Remarkably, this device achieves an ultrahigh mass loading of 23.51 mg cm<sup>-2</sup> and maintains fast ionic conductivity even at low temperature, offering a high capacitance of 3.44 F cm<sup>-2</sup>, and operates stably at an ultralow temperature of -60 °C. Interestingly, there are no capacitance decrease after cycling 10 000 times at low temperature [Fig. 10(c)], exhibiting its promising prospect in harsh environments application. Similarly, a proton conductive hydrogel electrolyte with an excellent conductivity of 1.51 mS cm<sup>-1</sup> was fabricated by utilizing the Grotthuss proton transport mechanism in Fig. 10(d).<sup>95</sup> When assembled into a pseudocapacitor, the device provides a high capacitance of 93.5 F g<sup>-1</sup> and can operate at -70 °C, showing outstanding prospects for low-temperature applications [Fig. 10(e)].

#### V. CONCLUSION AND PERSPECTIVES

The advantageous properties of the proton energy storage system present opportunities for energy storage device with high energy density and high-power density. In fact, research on proton-based supercapacitors has grown exponentially over the past decade. The development of electrode materials and manufacture methods has become the main means for the implementation of proton-based supercapacitors into practical applications. This review comprehensively summarizes the progress in electrode materials and proton storage mechanism. The key electrode materials for proton storage can be concluded as open-framework structure, layered structure, tunnel structure, and their energy storage mechanism are primarily surface redox reactions and intercalation processes. The proton-based flexible supercapacitors show promising advantage in energy storage: (1) High energy density and power energy: Protons can rapidly migrate by utilizing Grotthuss conduction network, which possesses a low migration barrier of 0.4 eV. (2) Long-cycle stability: Protons are the lightest and smallest ions, facilitating reversible electrode insertion without altering the electrode structure. (3) Anti-freezing properties: Acid electrolytes have a lower freezing point than other aqueous electrolytes, proving new ways for the design of energy storage device under extremely condition. (4) Flexible and low cost: The abundant sources of H<sup>+</sup> make it low cost and flexible in device design. Despite these benefits, several issues and challenges remain in material engineering, advanced characterization, and device design. To promote the rapid development of proton supercapacitors, the following research perspectives should be focused on.

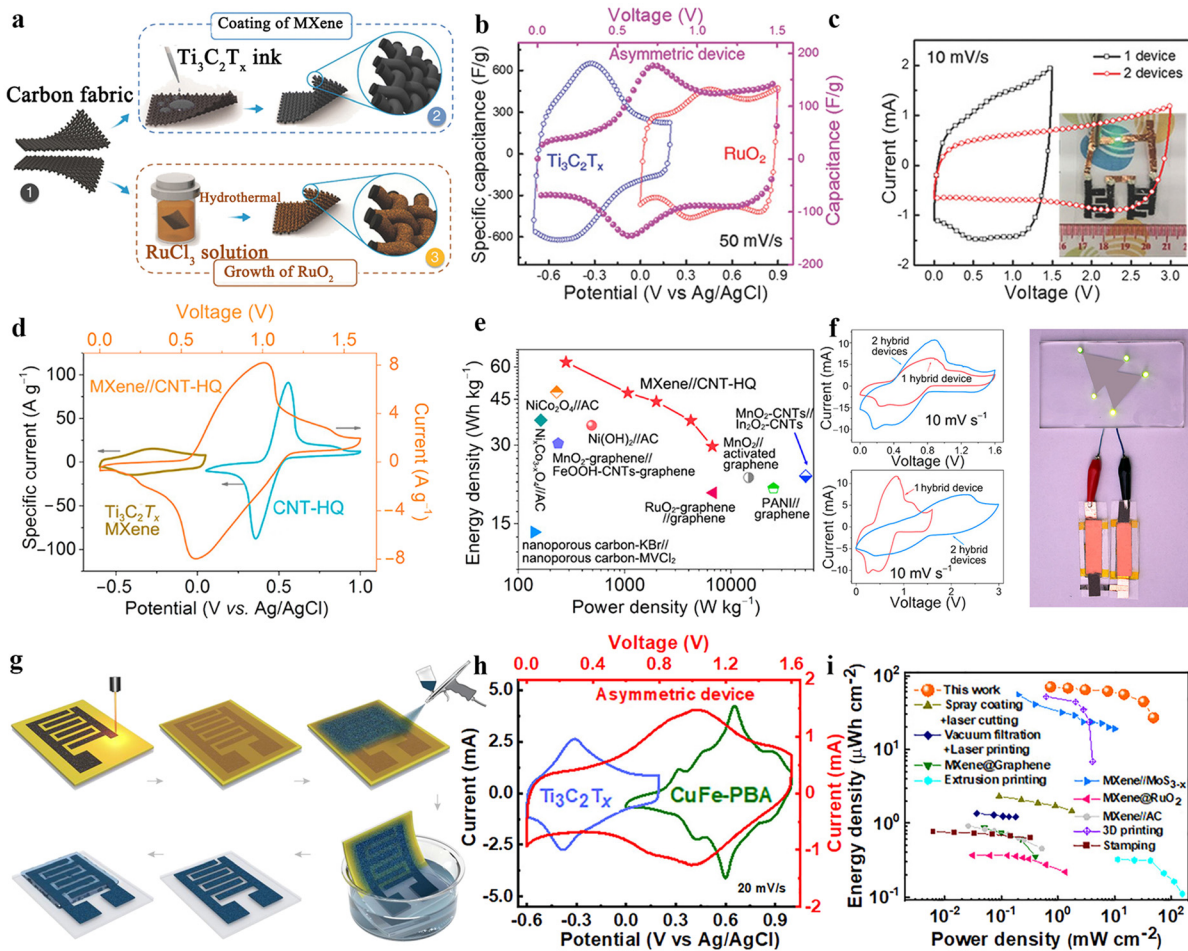


**FIG. 9.** Fabrication processes and electrochemical performance of proton-based flexible supercapacitors. (a) The schematic illustrations of the RuO<sub>2</sub>/Ti<sub>3</sub>C<sub>2</sub>T<sub>x</sub> flexible supercapacitor. The CV curves of (b) positive and negative electrode materials, and (c) integrated device, respectively. Reproduced with permission from Jiang et al., *Adv. Energy Mater.* **8**(13), 1703043 (2018). Copyright 2018 Wiley-VCH Verlag GmbH & Co.<sup>89</sup> (b) GaA. (d) CV curves, I Ragone plot, and (f) its practical application of CNT//MXene based supercapacitors. Reproduced with permission from Hu et al., *ACS Nano* **13**(6), 6899–6905 (2019). Copyright 2019 American Chemical Society.<sup>90</sup> The illustration of (g) fabrication process, (h) CV curves, and (i) Ragone plot of CuFePBA/Ti<sub>3</sub>C<sub>2</sub>T<sub>x</sub> based flexible supercapacitors. Reproduced with permission from Lei et al., *ACS Nano* **16** (2), 1974–1985 (2022). Copyright 2022 Authors, licensed under a Creative Commons Attribution (CC BY 4.0) License.<sup>93</sup>

First, it is vital to explore the electrode materials with outstanding proton storage capabilities. Various electrode materials have been developed for proton insertion. For instance, the PBAs and MXenes materials exhibit excellent rate properties because of the Grotthuss mechanism by utilizing their continuous hydrogen bonding networks. Therefore, designing materials such as WO<sub>3</sub> and RuO<sub>2</sub> with enhanced crystalline water networks to improve proton storage is a promising research direction. In addition, the metal oxides, including MoO<sub>3</sub>, V<sub>2</sub>O<sub>5</sub>, and WO<sub>3</sub>, have shown high energy density through pre-insertion of protons. The H<sup>+</sup> interstitial doping not only can improve proton diffusion kinetics but also can extend layer spacing, which will be a promising strategy for boosting proton storage. Finally, composites with conductive carbon materials can also promote proton conduction.

Another important scientific issue is the mechanism of proton storage. To clarify the structure changes and proton paths, advanced characterization techniques must be applied to further elucidate the structural changes and proton pathways. In recent years, many advanced characterization techniques have been used to investigate the proton storage processes, such as *in situ* FTIR,<sup>96</sup> *in situ* UV-vis spectroscopy,<sup>97</sup> and *in situ* electrochemical quartz crystal microbalance.<sup>98</sup> Researchers should reveal the issues related to capacitance fading and structural destroy in acid electrolyte. In addition, the first-principles investigation was carried out to understanding the intercalation/de-intercalation of protons in different layered structure materials.<sup>99</sup> Therefore, the contributions of *in situ* characterization methods and theoretical calculations can also promote to reveal the proton mechanism of electrode materials.

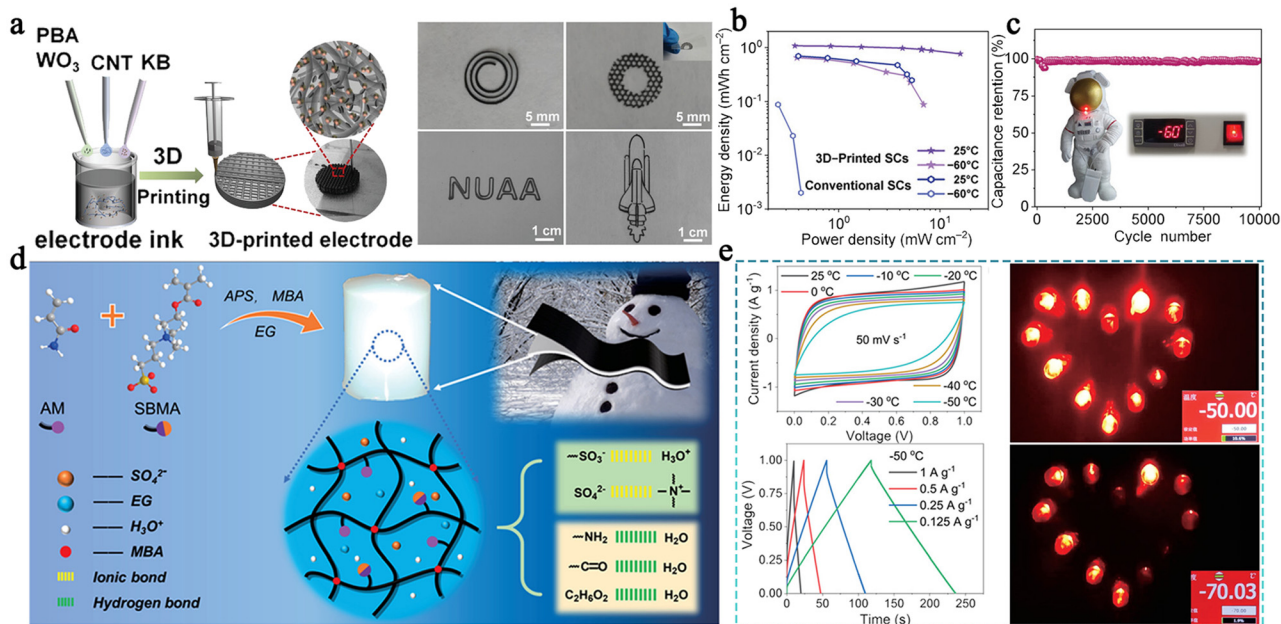


**FIG. 10.** Evaluating the performance and applications of proton-based flexible supercapacitors. (a) The schematic illustration of 3D-printing electrodes with various shapes, (b) Ragone plot of 3D-printing flexible supercapacitor, and (c) its cycling stability at  $-60^{\circ}\text{C}$ . Reproduced with permission from Zhang *et al.*, *Adv. Mater.* **35**, 2209963 (2023). Copyright 2023 Wiley-VCH Verlag GmbH & Co. KGaA.<sup>94</sup> (d) The fabrication process of anti-freezing electrolyte and (e) the CV, GCD curves, and applications of flexible supercapacitors at different temperatures. Reproduced with permission from Sun *et al.*, *Adv. Sci.* **9**(27), 2201679 (2022). Copyright 2022 Authors, licensed under a Creative Commons Attribution (CC BY) License.<sup>95</sup>

The challenge in assembling practical devices is lack of mature technology. Traditional manufacture techniques used to fabricate flexible supercapacitors, such as laser etching,<sup>100</sup> electrospinning,<sup>101</sup> and roll-to-roll,<sup>102</sup> have proven to be costly and wasteful of material. Printed electronics techniques offer a low-cost, large-scale, and customizable solution to solve the limitation of traditional manufacture methods in recent years to. Our group is dedicated to developing various types of printed flexible supercapacitors.<sup>103–106</sup> We have successfully formulated the carbon materials, metal oxides, and MOFs materials-based inks and printed them on different substrates (paper, cloth, and PET). This is a promising approach to fabricate flexible supercapacitors by using printing electronics technology, but challenges with printing accuracy and spatial resolution remain.

In conclusion, the proton storage represents a promising direction for electrochemical energy system, and printed electronics are an exciting technique for fabricating flexible supercapacitors for wearable electronic. Their further implementation is still addressing compatibility with manufacturing approaches and electrochemical performance. Obviously, the proton-based flexible supercapacitors will become a hot topic in future energy storage research due to their low cost and high performance.

## ACKNOWLEDGMENTS

This work was supported by the National Science Foundation of China (NSFC, Grant No. 52373252), the National High-level Talents Special Support Program, the Special Project on Knowledge

of Wuhan (No. whjkjsj027), the Fundamental Research Funds for the Central Universities (No. 2042022kf1052), and the China Postdoctoral Science Foundation (Nos. 2022TQ0239 and 2022M722465).

## AUTHOR DECLARATIONS

### Conflict of Interest

The authors have no conflicts to disclose.

### Author Contributions

**Jing Liang:** Project administration (equal); Writing – original draft (equal). **Wei Wu:** Project administration (equal); Writing – review & editing (equal).

## DATA AVAILABILITY

The data that support the findings of this study are available from the corresponding author upon reasonable request.

## REFERENCES

- C. Lethien, J. Le Bideau, and T. Brousse, *Energy Environ. Sci.* **12**(1), 96–115 (2019).
- H. M. Lee, S. Y. Choi, A. Jung, and S. H. Ko, *Angew. Chem., Int. Ed.* **52**(30), 7718–7723 (2013).
- J. Q. Zhao, J. J. Zha, Z. Y. Zeng, and C. L. Tan, *J. Mater. Chem. A* **9**(35), 18887–18905 (2021).

- <sup>4</sup>S. Butcha, C. Rajrjithong, V. Sattayarut, S. Youngjan, H. Nakajima, R. Supruangnet, J. Wittayakun, S. Prayoonpokarach, K. Faungnawakij, C. Chanthat, and P. Khemthong, *J. Energy Storage* **72**, 108578 (2023).
- <sup>5</sup>R. Colombo, N. Garino, D. Versaci, J. Amici, M. L. Para, E. Quartarone, C. Francia, F. Bella, and S. Bodoardo, *J. Mater. Sci.* **57**(33), 15690–15704 (2022).
- <sup>6</sup>R. Colombo, D. Versaci, J. Amici, F. Bella, M. L. Para, N. Garino, M. Laurenti, S. Bodoardo, and C. Francia, *Nanomaterial* **13**(14), 2149 (2023).
- <sup>7</sup>T. Zhu, S. Wang, Z. Q. Yu, H. C. Song, J. Xu, and K. J. Chen, *Small* **19**(33), 2301498 (2023).
- <sup>8</sup>Z. J. Zhang, X. Xiao, X. B. Zhu, and P. Tan, *Electrochem. Energy Rev.* **6**(1), 18 (2023).
- <sup>9</sup>E. Manarin, F. Corsini, S. Trano, L. Fagioli, J. Amici, C. Francia, S. Bodoardo, S. Turri, F. Bella, and G. Griffini, *ACS Appl. Polym. Mater.* **4**(5), 3855–3865 (2022).
- <sup>10</sup>L. Fagioli, D. Versaci, F. Di Berardino, J. Amici, C. Francia, S. Bodoardo, and F. Bella, *Batteries* **8**(11), 242 (2022).
- <sup>11</sup>I. Hasa, S. Mariappan, D. Saurel, P. Adelhelm, A. Y. Koposov, C. Masquelier, L. Croguennec, and M. Casas-Cabanas, *J. Power Sources* **482**, 228872 (2021).
- <sup>12</sup>Y. Z. Zhu, P. Y. Guan, R. B. Zhu, S. Zhang, Z. H. Feng, M. Y. Li, T. Wan, L. Hu, Y. J. Liu, Q. Li, J. Yu, and D. W. Chu, *J. Energy Chem.* **87**, 61–88 (2023).
- <sup>13</sup>M. Gandolfo, J. Amici, L. Fagioli, C. Francia, S. Bodoardo, and F. Bella, *Sustainable Mater. Technol.* **34**, e00504 (2022).
- <sup>14</sup>S. Trano, F. Corsini, G. Pascuzzi, E. Giove, L. Fagioli, J. Amici, C. Francia, S. Turri, S. Bodoardo, G. Griffini, and F. Bella, *ChemSusChem* **15**(12), e202200294 (2022).
- <sup>15</sup>R. T. Abdulwahid, S. B. Aziz, and M. F. Z. Kadir, *Mater. Today Sustainable* **23**, 100472 (2023).
- <sup>16</sup>J. Andrews, S. M. R. Niya, and R. Ojha, *Curr. Opin. Electrochem.* **31**, 100850 (2022).
- <sup>17</sup>T. Z. Xu, D. Wang, Z. W. Li, Z. Y. Chen, J. H. Zhang, T. S. Hu, X. G. Zhang, and L. F. Shen, *Nano-Micro Lett.* **14**(1), 126 (2022).
- <sup>18</sup>Y. K. Xu, X. Y. Wu, and X. L. Ji, *Small Struct.* **2**(5), 2000113 (2021).
- <sup>19</sup>M. R. Lukatskaya, S. Kota, Z. Lin, M.-Q. Zhao, N. Shpigel, M. D. Levi, J. Halim, P.-L. Taberna, M. W. Barsoum, P. Simon, and Y. Gogotsi, *Nat. Energy* **2**(8), 17105 (2017).
- <sup>20</sup>E. Makagon, O. Kraynis, R. Merkle, J. Maier, and I. Lubomirsky, *Adv. Funct. Mater.* **31**(50), 2104188 (2021).
- <sup>21</sup>H. Zhang, W. Wu, Q. Liu, F. Yang, X. Shi, X. Liu, M. Yu, and X. Lu, *Angew. Chem., Int. Ed.* **60**(2), 896–903 (2021).
- <sup>22</sup>G. J. Liang, F. N. Mo, X. L. Ji, and C. Y. Zhi, *Nat. Rev. Mater.* **6**(2), 109–123 (2021).
- <sup>23</sup>R. Epsztein, E. Shaulsky, M. Qin, and M. Elimelech, *J. Membr. Sci.* **580**, 316–326 (2019).
- <sup>24</sup>S. Wang, H. Jiang, Y. Dong, D. Clarkson, H. Zhu, C. M. Settens, Y. Ren, T. Nguyen, F. Han, W. Fan, S. Y. Kim, J. Zhang, W. Xue, S. K. Sandstrom, G. Xu, E. Tekoglu, M. Li, S. Deng, Q. Liu, S. G. Greenbaum, X. Ji, T. Gao, and J. Li, *Adv. Mater.* **34**(23), 2202063 (2022).
- <sup>25</sup>L. Vilčiauskas, M. E. Tuckerman, G. Bester, S. J. Paddison, and K.-D. Kreuer, *Nat. Chem.* **4**(6), 461–466 (2012).
- <sup>26</sup>C. X. Huang, W. Zhang, and W. T. Zheng, *Energy Storage Mater.* **61**, 102913 (2023).
- <sup>27</sup>H. Jiang, J. J. Hong, X. Wu, T. W. Surta, Y. Qi, S. Dong, Z. Li, D. P. Leonard, J. J. Holoubek, J. C. Wong, J. J. Razink, X. Zhang, and X. Ji, *J. Am. Chem. Soc.* **140**(37), 11556–11559 (2018).
- <sup>28</sup>C. G. Wang, S. S. Zhao, X. X. Song, N. N. Wang, H. L. Peng, J. Su, S. Y. Zeng, X. J. Xu, and J. Yang, *Adv. Energy Mater.* **12**(19), 2200157 (2022).
- <sup>29</sup>Z. Su, W. H. Ren, H. C. Guo, X. C. Peng, X. J. Chen, and C. Zhao, *Adv. Funct. Mater.* **30**(46), 2005477 (2020).
- <sup>30</sup>Y. K. Lv, J. C. Wang, D. W. Ji, J. H. Li, S. S. Zhao, Y. J. Zhao, Z. W. Cai, X. H. He, and X. F. Sun, *Front. Energy Res.* **10**, 957032 (2023).
- <sup>31</sup>F. Béguin, V. Presser, A. Balducci, and E. Frackowiak, *Adv. Mater.* **26**(14), 2219–2251 (2014).
- <sup>32</sup>D. Hulicova, J. Yamashita, Y. Soneda, H. Hatori, and M. Kodama, *Chem. Mater.* **17**(5), 1241–1247 (2005).
- <sup>33</sup>V. Barranco, A. Garcia-Gomez, M. Kunowsky, A. Linares-Solano, J. Ibanez, M. King, and J. M. Rojo, *J. Power Sources* **262**, 23–28 (2014).
- <sup>34</sup>A. Barua and A. Paul, *Energy Fuel* **35**(12), 10262–10273 (2021).
- <sup>35</sup>Z. Y. Song, L. Miao, L. Ruhlmann, Y. K. Lv, D. Z. Zhu, L. C. Li, L. H. Gan, and M. X. Liu, *Adv. Mater.* **33**(49), 2104148 (2021).
- <sup>36</sup>H. C. Yi, R. Z. Qin, S. X. Ding, Y. T. Wang, S. N. Li, Q. H. Zhao, and F. Pan, *Adv. Funct. Mater.* **31**(6), 2006970 (2021).
- <sup>37</sup>X. Y. Wu, J. J. Hong, W. Shin, L. Ma, T. C. Liu, X. X. Bi, Y. F. Yuan, Y. T. Qi, T. W. Surta, W. X. Huang, J. Neuefeind, T. P. Wu, P. A. Greaney, J. Lu, and X. L. Ji, *Nat. Energy* **4**(2), 123–130 (2019).
- <sup>38</sup>X. Y. Wu, S. Qiu, Y. K. Xu, L. Ma, X. X. Bi, Y. F. Yuan, T. P. Wu, R. Shahbazian-Yassar, J. Lu, and X. L. Ji, *ACS Appl. Mater. Interfaces* **12**(8), 9201–9208 (2020).
- <sup>39</sup>X. Peng, H. Guo, W. Ren, Z. Su, and C. Zhao, *Chem. Commun.* **56**(79), 11803–11806 (2020).
- <sup>40</sup>H. Jiang, W. Shin, L. Ma, J. J. Hong, Z. X. Wei, Y. S. Liu, S. Y. Zhang, X. Y. Wu, Y. K. Xu, Q. B. Guo, M. A. Subramanian, W. F. Stickle, T. P. Wu, J. Lu, and X. L. Ji, *Adv. Energy Mater.* **10**(28), 2000968 (2020).
- <sup>41</sup>X. Y. Dong, Z. W. Li, D. R. Luo, K. S. Huang, H. Dou, and X. G. Zhang, *Adv. Funct. Mater.* **33**(11), 2210473 (2023).
- <sup>42</sup>C. Ling, J. Chen, and F. Mizuno, *J. Phys. Chem. C* **117**(41), 21158–21165 (2013).
- <sup>43</sup>J. Guo, Y. Xu, S. Jin, L. Chen, T. Kaji, Y. Honsho, M. A. Addicoat, J. Kim, A. Saeki, H. Ihée, S. Seki, S. Irle, M. Hiramoto, J. Gao, and D. Jiang, *Nat. Commun.* **4**(1), 2736 (2013).
- <sup>44</sup>P. Bhanja, K. Bhunia, S. K. Das, D. Pradhan, R. Kimura, Y. Hijikata, S. Irle, and A. Bhaumik, *ChemSusChem* **10**(5), 921–929 (2017).
- <sup>45</sup>M. R. Biradar, C. R. K. Rao, S. V. Bhosale, and S. V. Bhosale, *Energy Fuel* **37**(6), 4671–4681 (2023).
- <sup>46</sup>S. Chandra, D. Roy Chowdhury, M. Addicoat, T. Heine, A. Paul, and R. Banerjee, *Chem. Mater.* **29**(5), 2074–2080 (2017).
- <sup>47</sup>Y. Yang, P. Zhang, L. Hao, P. Cheng, Y. Chen, and Z. Zhang, *Angew. Chem., Int. Ed.* **60**(40), 21838–21845 (2021).
- <sup>48</sup>A. Jadon, S. Prabhudev, G. Buvat, S. G. Patnaik, M. Djafari-Rouhani, A. Estève, D. Guay, and D. Pech, *ACS Appl. Energy Mater.* **3**(5), 4144–4148 (2020).
- <sup>49</sup>A. Mukhopadhyay, Y. Jiao, R. Katahira, P. N. Ciesielski, M. Himmel, and H. Zhu, *Nano Lett.* **17**(12), 7897–7907 (2017).
- <sup>50</sup>H. Yao, F. Zhang, G. Zhang, H. Luo, L. Liu, M. Shen, and Y. Yang, *Chem. Eng. J.* **334**, 2547–2557 (2018).
- <sup>51</sup>X. Liu, S. Chen, Z. Xiong, K. Li, and Y. Zhang, *Prog. Mater.* **130**, 100978 (2022).
- <sup>52</sup>B. Gerand, G. Nowogrocki, J. Guenot, and M. Figlarz, *J. Solid State Chem.* **29**(3), 429–434 (1979).
- <sup>53</sup>W. Sun, M. T. Yeung, A. T. Lech, C.-W. Lin, C. Lee, T. Li, X. Duan, J. Zhou, and R. B. Kaner, *Nano Lett.* **15**(7), 4834–4838 (2015).
- <sup>54</sup>J. Besnardiere, B. Ma, A. Torres-Pardo, G. Walley, H. Kabbour, J. M. González-Calbet, H. J. Von Bardeleben, B. Fleury, V. Buissette, C. Sanchez, T. Le Mercier, S. Cassaignon, and D. Portehault, *Nat. Commun.* **10**(1), 327 (2019).
- <sup>55</sup>X. D. Liu, Q. Yang, L. Yuan, D. J. Qi, X. J. Wei, X. W. Zhou, S. F. Chen, L. H. Cao, Y. Zeng, J. Z. Jia, and C. Y. Wang, *Chem. Eng. J.* **425**, 131431 (2021).
- <sup>56</sup>Z. Chen, Y. Peng, F. Liu, Z. Le, J. Zhu, G. Shen, D. Zhang, M. Wen, S. Xiao, C.-P. Liu, Y. Lu, and H. Li, *Nano Lett.* **15**(10), 6802–6808 (2015).
- <sup>57</sup>S. H. You, S. M. Jung, J. Park, J. Kim, J. K. Kim, J. Son, and Y. T. Kim, *Sci. Adv.* **9**(39) (2023).
- <sup>58</sup>J. B. Mitchell, W. C. Lo, A. Genc, J. LeBeau, and V. Augustyn, *Chem. Mater.* **29**(9), 3928–3937 (2017).
- <sup>59</sup>R. Wang, J. B. Mitchell, Q. Gao, W.-Y. Tsai, S. Boyd, M. Pharr, N. Balke, and V. Augustyn, *ACS Nano* **12**(6), 6032–6039 (2018).
- <sup>60</sup>J. B. Mitchell, N. R. Geise, A. R. Paterson, N. C. Osti, Y. Sun, S. Fleischmann, R. Zhang, L. A. Madsen, M. F. Toney, D. Jiang, A. I. Kolesnikov, E. Mamontov, and V. Augustyn, *ACS Energy Lett.* **4**(12), 2805–2812 (2019).
- <sup>61</sup>M. S. Zhu, W. J. Meng, Y. Huang, Y. Huang, and C. Y. Zhi, *ACS Appl. Mater. Interfaces* **6**(21), 18901–18910 (2014).
- <sup>62</sup>I. A. de Castro, R. S. Datta, J. Z. Ou, A. Castellanos-Gomez, S. Sriram, T. Daeneke, and K. Kalantar-zadeh, *Adv. Mater.* **29**(40), 1701619 (2017).

- <sup>63</sup>Q. Mahmood, W. S. Kim, and H. S. Park, *Nanoscale* **4**(24), 7855–7860 (2012).
- <sup>64</sup>X. Wang, Y. Xie, K. Tang, C. Wang, and C. Yan, *Angew. Chem., Int. Ed.* **57**(36), 11569–11573 (2018).
- <sup>65</sup>H. Guo, D. Goonetilleke, N. Sharma, W. Ren, Z. Su, A. Rawal, and C. Zhao, *Cell Rep. Phys. Sci.* **1**(10), 100225 (2020).
- <sup>66</sup>L. Yan, J. Huang, Z. Guo, X. Dong, Z. Wang, and Y. Wang, *ACS Energy Lett.* **5**(2), 685–691 (2020).
- <sup>67</sup>W. Wang, Y. Jiang, Y. Yang, F. Xiong, S. Zhu, J. Wang, L. Du, J. Chen, L. Cui, J. Xie, Q. An, and L. Mai, *ACS Nano* **16**(10), 17097–17106 (2022).
- <sup>68</sup>X. Hou, M. Ruan, L. Zhou, J. Wu, B. Meng, W. Huang, K. Zhong, K. Yang, Z. Fang, and K. Xie, *J. Energy Chem.* **78**, 91–101 (2023).
- <sup>69</sup>W. Xu, K. Zhao, X. Liao, C. Sun, K. He, Y. Yuan, W. Ren, J. Li, T. Li, C. Yang, H. Cheng, Q. Sun, I. Manke, X. Lu, and J. Lu, *J. Am. Chem. Soc.* **144**(38), 17407–17415 (2022).
- <sup>70</sup>W. Liu, Z. Zhang, J. Shi, Y. Zheng, Y. Wu, X. Fu, N. Liu, J. Su, and Y. Gao, *J. Mater. Chem. A* **10**(8), 4043–4052 (2022).
- <sup>71</sup>W. Huang, K. Zhang, B. Yuan, L. Yang, and M. Zhu, *Energy Storage Mater.* **50**, 152–160 (2022).
- <sup>72</sup>J. Dai, X. Qi, L. Xia, Q. Xue, L. Luo, X. Wang, C. Yang, D. Li, H. Xie, A. Cabot, L. Dai, and Y. Xu, *Adv. Funct. Mater.* **33**(10), 2212440 (2023).
- <sup>73</sup>Q. Zhao, L. Liu, J. Yin, J. Zheng, D. Zhang, J. Chen, and L. A. Archer, *Angew. Chem., Int. Ed.* **59**(8), 3048–3052 (2020).
- <sup>74</sup>Q. Pan, R. Dong, H. Lv, X. Sun, Y. Song, and X.-X. Liu, *Chem. Eng. J.* **419**, 129491 (2021).
- <sup>75</sup>M. Naguib, M. Kurtoglu, V. Presser, J. Lu, J. Niu, M. Heon, L. Hultman, Y. Gogotsi, and M. W. Barsoum, *Adv. Mater.* **23**(37), 4248–4253 (2011).
- <sup>76</sup>J. Li, H. Wang, and X. Xiao, *Energy Environ. Mater.* **3**(3), 306–322 (2020).
- <sup>77</sup>M. R. Lukatskaya, S.-M. Bak, X. Yu, X.-Q. Yang, M. W. Barsoum, and Y. Gogotsi, *Adv. Energy Mater.* **5**(15), 1500589 (2015).
- <sup>78</sup>X. Mu, D. Wang, F. Du, G. Chen, C. Wang, Y. Wei, Y. Gogotsi, Y. Gao, and Y. Dall’Agnese, *Adv. Funct. Mater.* **29**(29), 1902953 (2019).
- <sup>79</sup>M. Hu, T. Hu, Z. Li, Y. Yang, R. Cheng, J. Yang, C. Cui, and X. Wang, *ACS Nano* **12**(4), 3578–3586 (2018).
- <sup>80</sup>J. Wen, Q. Fu, W. Wu, H. Gao, X. Zhang, and B. Wang, *ACS Appl. Mater. Interfaces* **11**(7), 7087–7095 (2019).
- <sup>81</sup>Y. Sun, C. Zhan, P. R. C. Kent, M. Naguib, Y. Gogotsi, and D. Jiang, *ACS Appl. Mater. Interfaces* **12**(1), 763–770 (2020).
- <sup>82</sup>H. Shao, K. Xu, Y.-C. Wu, A. Iadecola, L. Liu, H. Ma, L. Qu, E. Raymundo-Piñero, J. Zhu, Z. Lin, P.-L. Taberna, and P. Simon, *ACS Energy Lett.* **5**(9), 2873–2880 (2020).
- <sup>83</sup>M. Brunet Cabré, D. Spurling, P. Martinuz, M. Longhi, C. Schröder, H. Nolan, V. Nicolosi, P. E. Colavita, and K. McKelvey, *Nat. Commun.* **14**(1), 374 (2023).
- <sup>84</sup>X. Zhao, Q. Liu, C. Zhong, Y. Li, Q. Chen, D. Chao, and M. Chen, *Adv. Funct. Mater.* **32**(43), 2205874 (2022).
- <sup>85</sup>Z. Qin, Y. Song, Y. Liu, and X.-X. Liu, *Energy Storage Mater.* **53**, 569–579 (2022).
- <sup>86</sup>N. An, Z. Guo, C. Guo, M. Q. Wei, D. M. Sun, Y. Y. He, W. L. Li, L. Zhou, Z. A. Hu, and X. Y. Dong, *Chem. Eng. J.* **458**, 141434 (2023).
- <sup>87</sup>X. Gao, H. Wu, C. Su, C. Lu, Y. Dai, S. Zhao, X. Hu, F. Zhao, W. Zhang, I. P. Parkin, C. J. Carmalt, and G. He, *Energy Environ. Sci.* **16**(4), 1364–1383 (2023).
- <sup>88</sup>Z. Li, J. Tan, Y. Wang, C. Gao, Y. Wang, M. Ye, and J. Shen, *Energy Environ. Sci.* **16**, 2398–2431 (2023).
- <sup>89</sup>Q. Jiang, N. Kurra, M. Alhabeb, Y. Gogotsi, and H. N. Alshareef, *Adv. Energy Mater.* **8**(13), 1703043 (2018).
- <sup>90</sup>M. Hu, C. Cui, C. Shi, Z.-S. Wu, J. Yang, R. Cheng, T. Guang, H. Wang, H. Lu, and X. Wang, *ACS Nano* **13**(6), 6899–6905 (2019).
- <sup>91</sup>T. Z. Xu, Z. W. Li, D. Wang, M. R. Zhang, L. F. Ai, Z. Y. Chen, J. H. Zhang, X. G. Zhang, and L. F. Shen, *Adv. Funct. Mater.* **32**(5), 2107720 (2022).
- <sup>92</sup>X. Xiao, T. Ding, L. Yuan, Y. Shen, Q. Zhong, X. Zhang, Y. Cao, B. Hu, T. Zhai, L. Gong, J. Chen, Y. Tong, J. Zhou, and Z. L. Wang, *Adv. Energy Mater.* **2**(11), 1328–1332 (2012).
- <sup>93</sup>Y. Lei, W. Zhao, Y. Zhu, U. Buttner, X. Dong, and H. N. Alshareef, *ACS Nano* **16**(2), 1974–1985 (2022).
- <sup>94</sup>M. R. Zhang, T. Z. Xu, D. Wang, T. Y. Yao, Z. M. Xu, Q. S. Liu, L. F. Shen, and Y. Yu, *Adv. Mater.* **35**, 2209963 (2023).
- <sup>95</sup>W. G. Sun, Z. Xu, C. D. Qiao, B. X. Lv, L. G. Gai, X. X. Ji, H. H. Jiang, and L. B. Liu, *Adv. Sci.* **9**(27), 2201679 (2022).
- <sup>96</sup>M. Shi, R. Wang, L. Li, N. Chen, P. Xiao, C. Yan, and X. Yan, *Adv. Funct. Mater.* **33**(1), 2209777 (2023).
- <sup>97</sup>L. Åkerlund, R. Emanuelsson, G. Hernández, F. Ruipérez, N. Casado, D. Brandell, M. Strømme, D. Mecerreyes, and M. Sjödin, *ACS Appl. Energy Mater.* **2**(6), 4486–4495 (2019).
- <sup>98</sup>B. Gavriel, G. Bergman, M. Turgeman, A. Nimkar, Y. Elias, M. D. Levi, D. Sharon, N. Shpigel, and D. Aurbach, *Mater. Today Energy* **31**, 101189 (2023).
- <sup>99</sup>S. Posada-Pérez, G.-M. Rignanese, and G. Hautier, *Chem. Mater.* **33**(17), 6942–6954 (2021).
- <sup>100</sup>H. Choi, P. T. Nguyen, and J. B. In, *Appl. Surf. Sci.* **483**, 481–488 (2019).
- <sup>101</sup>L. A. Mercante, R. S. Andre, M. H. M. Facure, D. S. Correa, and L. H. C. Mattoso, *Chem. Eng. J.* **465**, 142847 (2023).
- <sup>102</sup>Z. Gao, C. Bumgardner, N. N. Song, Y. Y. Zhang, J. J. Li, and X. D. Li, *Nat. Commun.* **7**, 11586 (2016).
- <sup>103</sup>J. Liang, Y. Feng, L. Liu, S. Q. Li, C. Z. Jiang, and W. Wu, *J. Mater. Chem. A* **7**(26), 15960–15968 (2019).
- <sup>104</sup>J. Liang, C. Z. Jiang, and W. Wu, *Appl. Phys. Rev.* **8**(2), 021319 (2021).
- <sup>105</sup>J. Liang, B. Tian, S. Q. Li, C. Z. Jiang, and W. Wu, *Adv. Energy Mater.* **10**(12), 2000022 (2020).
- <sup>106</sup>L. Liu, Y. Feng, and W. Wu, *J. Power Sources* **410–411**, 69–77 (2019).